

Copyright © 1982, by the author(s).
All rights reserved.

Permission to make digital or hard copies of all or part of this work for personal or classroom use is granted without fee provided that copies are not made or distributed for profit or commercial advantage and that copies bear this notice and the full citation on the first page. To copy otherwise, to republish, to post on servers or to redistribute to lists, requires prior specific permission.

A COMPUTER-ASSISTED STUDY OF
FORCED RELAXATION OSCILLATIONS

by

T.S. Parker and L.O. Chua

Memorandum No. UCB/ERL M82/81

5 November 1982

ELECTRONICS RESEARCH LABORATORY
College of Engineering
University of California, Berkeley
94720

**A Computer-Assisted Study
of
Forced Relaxation Oscillations[†]**

Thomas S. Parker

Leon O. Chua[‡]

ABSTRACT

A piecewise linear version of the forced relaxation oscillator is studied. Computer results are discussed and informal explanations of some properties of the subharmonic solutions are given. The experimental results display a unique interrelationship between the subharmonics in that all subharmonics can be decomposed into a fundamental set containing the odd order, single loop subharmonics.

[†]Research supported in part by the Hertz Foundation, by the Office of Naval Research under Contract N00014-76-C-0572, by the National Science Foundation under Grants ECS 80-20-640/ENG-7722745, and by the Joint Services Electronics Program Contract F49620-79-C-0178.

[‡]The authors are with the Department Of Electrical Engineering and Computer Sciences and the Electronics Research Laboratory, University of California, Berkeley, CA 94720.

1. Introduction

1.1. Selected History

The classical forced relaxation oscillation equation is the van der Pol equation:

$$\epsilon \ddot{x} + (x^2 - 1)\dot{x} + \epsilon x = b \cos(\omega t). \quad (1.1)$$

In 1949 Levinson[1] attacked this equation analytically by replacing the cubic nonlinearity with a piecewise linear one. Considering the problem for ϵ small, he proved that for some intervals of b the equation exhibits random behavior. For these same intervals of b he also proved the existence of a closed interval of rotation numbers two of which are stable. The interval of rotation numbers has the form $[1/(2n+1), 1/(2n-1)]$ where n is a large integer. The endpoints of the interval are the two stable rotation numbers.

More recently Levi[2] expanded this result. He used a smooth nonlinearity required to be close to a piecewise linear characteristic and he also replaced the sinusoidal forcing function with a smooth function close to a square wave. For ϵ small and fixed, Levi proved the b axis is divided into intervals of which there are three types:

- A-type where a single, stable subharmonic exists;
- B-type where two stable subharmonics (plus random behavior) exist;
- g-type where bifurcations occur.

Levi's B-type intervals correspond to the intervals of b found by Levinson. The A- and B-type intervals alternate and are separated by the g-type intervals which are small and do not concern us.

1.2. The Purpose of the Paper

The purpose of this paper is threefold. The initial motivation was to obtain accurate data on the different behaviors displayed by a van der Pol type equation. High accuracy is essential since systems which exhibit stochastic behavior are, by their very nature, extremely sensitive to small perturbations. To this end a piecewise linear approach was chosen. The advantage of using piecewise linear analysis over standard integration techniques is that error does not accumulate at each point where the trajectory is evaluated—error only accumulates when the Region boundaries are crossed. Hence the results presented here are the most accurate ever obtained

for a forced relaxation oscillator. For a further discussion on accuracy consult **Appendix I**.

The second reason for this paper is Levi's paper. He proved what types of behavior are possible and how this behavior is structured as b is varied. His results are a major breakthrough yet they are theoretical in nature—they leave some quantitative questions unanswered. How small must ϵ be? How do the lengths of the A-type and B-type intervals depend on ϵ and b ? This paper answers some questions of this type as well as numerically verifying some of Levi's results.

Since Levinson's and Levi's papers contain mathematical proofs of difficult theorems, it is not easy to obtain an intuitive understanding of forced relaxation oscillations from them. The main purpose of this paper is to give that intuitive understanding. A state space approach is used to explain the existence of subharmonics, intervals of rotation numbers, and random behavior. Using evidence gathered from computer simulations we show that the different subharmonic solutions of the piecewise linear relaxation oscillation equation are intimately related and can be decomposed into a fundamental set of subharmonics.

1.3. The Circuit and the Equation

Consider the circuit in Figure 1(a). The equation governing the current is

$$\ddot{i} + \frac{1}{L}f'(i)i + \frac{1}{LC}i = \frac{A\omega}{L}\cos(\omega t) \quad (1.2)$$

where $\dot{}$ indicates $\frac{d}{dt}$.

It is standard to normalize differential equations to have dimensionless time. By defining $\omega_0 := 1/\sqrt{LC}$, $t' := \omega_0 t$, and $\omega' := \omega/\omega_0$, (1.2) becomes

$$\sqrt{L/C} \frac{d^2 i}{dt'^2} + f'(i) \frac{di}{dt'} + \sqrt{L/C} i = A\omega' \cos(\omega' t'). \quad (1.3)$$

Next define

$$\epsilon := \sqrt{L/C} \quad (1.4.a)$$

and

$$b := A\omega' \quad (1.4.b)$$

to get

$$\epsilon \frac{d^2 i}{dt^2} + f'(i) \frac{di}{dt} + \epsilon i = b \cos(\omega' t'). \quad (1.5)$$

Equations (1.4) will be useful later since they allow us to relate our results (with dimensioned time) to previous work.

For $f(i) = (1/3)i^3 - i$ (Figure 1(b)) (1.5) becomes the van der Pol equation. We consider the case where the resistor characteristic is the three-segment, piecewise linear curve in Figure 1(c). The vertical lines $i = \pm I_0$ split the i - v plane into three Regions. The Regions are numbered from right to left. The subscript i (ranging from one to three) will be used to denote a Region dependent value. Within each Region (1.2) reduces to a linear equation.

To apply state space techniques, choose i_L and v_C as state variables and rewrite (1.2) as

$$\begin{bmatrix} \dot{i}_L \\ \dot{v}_C \end{bmatrix} = \begin{bmatrix} -\frac{R_i}{L} & \frac{1}{L} \\ \frac{-1}{C} & 0 \end{bmatrix} \begin{bmatrix} i_L \\ v_C \end{bmatrix} + \begin{bmatrix} \frac{A \sin(\omega t) - V_{oi}}{L} \\ 0 \end{bmatrix} \quad (1.6)$$

where R_i and V_{oi} are the slope and y-intercept of the line lying on the i th segment of the resistor characteristic. Equation (1.6) is the one we consider in this paper. To simulate the relaxation oscillation equation we require $R_1 = R_3 > 0$, $R_2 < 0$ and $V_{o2} = 0$.

We should mention here how Levinson's and Levi's choice of variables relates to ours. Levinson's x_1 and Levi's x both correspond to our i_L . Their second variable (x_2 and y , respectively) is equal to the sum of v_C and the voltage source¹. v_C is a more natural choice of state variable than $v_C + A \sin(\omega t)$ and, since our goal is to gain physical intuition, we will use v_C as a state variable even though it may appear inconvenient to do so.

2. The Autonomous Case

The solution of (1.6) with $A = 0$ is

$$\begin{bmatrix} i_L \\ v_C \end{bmatrix} = v_{1i} e^{s_{1i}(t-t_0)} + v_{2i} e^{s_{2i}(t-t_0)} + \begin{bmatrix} 0 \\ V_{oi} \end{bmatrix} \quad (2.1)$$

where $\alpha_i := -R_i/2L$, $\beta_i := \sqrt{\alpha_i^2 - \omega_0^2}$, $s_{1i} := \alpha_i + \beta_i$, $s_{2i} := \alpha_i - \beta_i$ and the eigenvectors are

¹Remember that Levi does not use a sinusoid as a driving function. He states that this discrepancy should make little difference in the behavior of the system.

$$v_{1i} = \frac{i_L(t_0) + s_{2i}C(v_C(t_0) - V_{oi})}{s_{1i} - s_{2i}} \begin{bmatrix} s_{1i} \\ -1/C \end{bmatrix}$$

and

$$v_{2i} = \frac{i_L(t_0) + s_{1i}C(v_C(t_0) - V_{oi})}{s_{1i} - s_{2i}} \begin{bmatrix} -s_{2i} \\ 1/C \end{bmatrix}.$$

We only consider the case where s_{1i} and s_{2i} are real since it is only for real eigenvalues that relaxation oscillations occur.

The following three sections explain the dynamics of each Region separately by extending, in turn, each segment of the resistor characteristic into the whole i - v plane. To simplify the explanations we assume L is small. This assumption corresponds to small ϵ .

2.1. Region I

In Region I, $R_1 > 0$, hence $\alpha_1 < 0$ and $s_{21} < s_{11} < 0$. The approximations for L small are $s_{11} = -1/R_1C$, $s_{21} = -R_1/L$,

$$v_{11} = \begin{bmatrix} \frac{v_C(t_0) - V_{o1}}{R_1} \\ v_C(t_0) - V_{o1} \end{bmatrix} \text{ and } v_{21} = \begin{bmatrix} i_L(t_0) - \frac{v_C(t_0) - V_{o1}}{R_1} \\ 0 \end{bmatrix}. \quad (2.2)$$

Consult **Appendix II** for details on the approximations used.

The slow eigenvector v_{11} lies along the resistor characteristic while the fast eigenvector v_{21} is horizontal². Note that the fast eigenvalue tends to $-\infty$ as $L \rightarrow 0$. Thus, for any initial condition not on the resistor characteristic, the initial motion is a rapid horizontal jump to the resistor characteristic (Figure 2(a)). Once the component due to the fast eigenvector has died out, the trajectory exponentially decays along the resistor characteristic at the slow rate which is independent of L . Region I is stable and all trajectories tend toward the node at $(0, V_{o1})$ as $t \rightarrow \infty$.

Note that once $v_{21}e^{s_{21}(t-t_0)}$ becomes negligible (which occurs very quickly for small L) the dynamics in Region I are essentially one-dimensional—the subsequent motion occurs only along v_{11} . This reduction of the system to one dimension is a major reason analytical results have been obtained for small ϵ .

²We define the slow eigenvalue as the one with the lesser absolute value. The remaining eigenvalue is the fast one. We define the slow (fast) eigenvector as the eigenvector associated with the slow (fast) eigenvalue.

2.2. Region II

Here $R_2 < 0$ forcing $\alpha_2 > 0$ and $s_{12} > s_{22} > 0$. Region II is unstable with a node at the origin. The approximations for L small are $s_{12} = -R_2/L$, $s_{22} = -1/R_2C$,

$$v_{12} = \begin{bmatrix} i_L(t_0) - \frac{v_C(t_0)}{R_2} \\ 0 \end{bmatrix} \text{ and } v_{22} = \begin{bmatrix} \frac{v_C(t_0)}{R_2} \\ v_C(t_0) \end{bmatrix}. \quad (2.3)$$

As in Region I the slow eigenvector v_{22} lies along the resistor characteristic and the fast eigenvector v_{12} is nearly horizontal. Any trajectory with an initial condition not on the resistor characteristic will move horizontally and very rapidly away from the resistor characteristic (Figure 2(b)). Again we see a reduction of the system to one dimension.

2.3. Region III

Due to symmetry, Region III behaves identically to Region I except the stable node is $(0, V_{o3})$.

2.4. Regions I, II and III Combined

Figure 2(c) shows a phase portrait for the entire system obtained by joining the phase portraits of the three different Regions. Due to the expanding nature of Region II and the contracting nature of Regions I and III, it can be shown that all trajectories tend toward a unique, stable limit cycle[3]. Examples are shown in Figure 3.

Notice the limit cycle looks like a parallelogram for small ϵ . The horizontal segments of the parallelogram are traversed very quickly; in fact, as this plot was being made, the motion appeared to be instantaneous. As ϵ increases the slopes of the slow eigenvectors decrease and the sides of the limit cycle move away from the resistor characteristic. Also as ϵ increases, the fast eigenvalues decrease and the slopes of the fast eigenvectors increase. This causes the limit cycle to become more rounded. As $\epsilon \rightarrow \infty$ the system becomes lossless and the limit cycle becomes an ellipse.

3. The Nonautonomous Case

3.1. The Exact Solution

With $A \neq 0$ the solution of (1.6) is the sum of the autonomous solution (2.1) and the contribution from the forcing function which consists of a transient and a steady state term³:

$$\begin{aligned}
 \begin{bmatrix} i_L \\ v_C \end{bmatrix} &= v_{1i} e^{s_{1i}(t-t_0)} + v_{2i} e^{s_{2i}(t-t_0)} + \begin{bmatrix} 0 \\ V_{oi} \end{bmatrix} \\
 &+ \frac{1}{s_{1i} - s_{2i}} \left[\begin{array}{l} \frac{As_{1i} e^{s_{1i}(t-t_0)}}{L\sqrt{s_{1i}^2 + \omega^2}} \cos(\omega t_0 + \phi_{1i}) - \frac{As_{2i} e^{s_{2i}(t-t_0)}}{L\sqrt{s_{2i}^2 + \omega^2}} \cos(\omega t_0 + \phi_{2i}) \\ - \frac{A\omega_0^2 e^{s_{1i}(t-t_0)}}{\sqrt{s_{1i}^2 + \omega^2}} \cos(\omega t_0 + \phi_{1i}) + \frac{A\omega_0^2 e^{s_{2i}(t-t_0)}}{\sqrt{s_{2i}^2 + \omega^2}} \cos(\omega t_0 + \phi_{2i}) \end{array} \right] \\
 &+ \frac{A}{L\sqrt{(s_{1i}^2 + \omega^2)(s_{2i}^2 + \omega^2)}} \begin{bmatrix} \omega \sin(\omega t + \theta_i) \\ (1/C) \cos(\omega t + \theta_i) \end{bmatrix}
 \end{aligned} \tag{3.1}$$

where $\phi_{ji} := \text{Tan}^{-1}(-s_{ji}/\omega)$ for $j=1,2$; $\theta_i := \arg(-2\alpha_i\omega + j(\omega_0^2 - \omega^2))$ and α_i and β_i are defined after equation (2.1). The $\arg(z)$ notation denotes the angle of the complex number z and is used since θ_i may occur in any quadrant and Tan^{-1} only gives answers in quadrants I and IV.

To understand the behavior of (3.1) we will simplify it in two steps. The first step is to consider small L (corresponding to small ϵ). The second is to consider ω large. The reason for the second assumption will be given when we do it.

3.2. The Solution for Small L

For L small, (3.1) can be approximated by

$$\begin{aligned}
 \begin{bmatrix} i_L \\ v_C \end{bmatrix} &= \left\{ v_C(t_0) - V_{oi} - \frac{A \cos(\omega t_0 + \phi_{1i})}{\sqrt{1 + (\omega R_i C)^2}} \right\} \begin{bmatrix} 1/R_i \\ 1 \end{bmatrix} e^{-\frac{t-t_0}{R_i C}} \\
 &+ \left\{ R_i i_L(t_0) - v_C(t_0) - V_{oi} - A \sin(\omega t_0) \right\} \begin{bmatrix} 1/R_i \\ 0 \end{bmatrix} e^{-\frac{t-t_0}{L/R_i}} \\
 &+ \begin{bmatrix} 0 \\ V_{oi} \end{bmatrix} + \frac{A}{\sqrt{1 + (\omega R_i C)^2}} \begin{bmatrix} \omega C \sin(\omega t + \theta_i) \\ \cos(\omega t + \theta_i) \end{bmatrix}
 \end{aligned} \tag{3.2}$$

where $\phi_{1i} := \text{Tan}^{-1}(1/\omega R_i C)$ and $\theta_i := \arg(\omega R_i C + j)$. For details on the approximations involved, see **Appen-**

³Derivation of this solution is straightforward, but very messy.

dix II. Notice that the slow eigenvector still lies along the resistor characteristic and the fast eigenvector is still horizontal. The main qualitative difference between the nonautonomous and the autonomous solutions is the sinusoidal terms. The system is still in some sense one dimensional.

3.3. The Solution for Small L and Large ω

Equation (1.5) is the dimensionless form of the relaxation oscillation equation and is the version that Levinson and Levi studied. In their work dimensionless frequency is held constant. The relation between dimensioned frequency ω and dimensionless frequency ω' is $\omega = \omega' \omega_0 = \omega' / \sqrt{LC}$. Thus constant ω' implies that as $L \rightarrow 0$, $\omega \rightarrow \infty$. For ω large (3.2) can be approximated by (see Appendix II)

$$\begin{aligned} \begin{bmatrix} i_L \\ v_C \end{bmatrix} &= \begin{bmatrix} \frac{v_C(t_0) - V_{oi}}{R_i} \\ v_C(t_0) - V_{oi} \end{bmatrix} e^{-\frac{t-t_0}{R_i C}} + \begin{bmatrix} i_L(t_0) - \frac{v_C(t_0) - V_{oi} + A \sin(\omega t_0)}{R_i} \\ 0 \end{bmatrix} e^{-\frac{t-t_0}{L/R_i}} \\ &+ \begin{bmatrix} \frac{A}{R_i} \sin(\omega t) \\ V_{oi} \end{bmatrix}. \end{aligned} \quad (3.3)$$

Note that v_C has simplified to the *autonomous* solution and i_L is the *autonomous* solution with two extra terms. One term is a steady state sine wave and the other is an additional term in the coefficient of the fast exponent.

3.4. The Dynamics of Each Region for Small L and Large ω

In Region I the motion described by equation (3.3) is the same as the autonomous case except for the sinusoidal variations in i_L . The initial motion is a quick horizontal jump toward the resistor characteristic. Following this initial jump, the trajectory straddles the resistor characteristic and slides down it toward $(0, V_{oi})$ always oscillating horizontally (see Figure 4(a)). Note how the trajectory bunches up as it travels down the characteristic. This is due to the exponential decay of the autonomous components of v_C and i_L . The behavior in Region II is quick and horizontal. The behavior in Region III is the same as in Region I except for the shift in the resistor characteristic (see Figure 4(b)).

Under the assumptions of small L and large ω the dynamics of each Region are simple enough. It is clear that the key to the variety of behavior exhibited by the relaxation oscillation equation must lie in the boundary crossings.

3.5. The Boundary Crossing

Consider a trajectory crossing from Region I to Region II. Region II is entered when $i_L(t) = I_o$. Let t' denote the time when this occurs and let $v'_C := v_C(t')$. Then I_o , v'_C and t' are the initial conditions for Region II. One of two things can happen after entering Region II: the trajectory may cross Region II and enter Region III or the trajectory may turn and reenter Region I.

We can get a good idea of which route the trajectory follows by examining the i_L component of the fast eigenvector in Region II (hereafter called the fast i_L term). Imagine Region II extended to the whole i - v plane. If the fast i_L term is positive, then $i_L \rightarrow +\infty$ as $t \rightarrow \infty$. If it is negative, then $i_L \rightarrow -\infty$ as $t \rightarrow \infty$. Hence the fast i_L term predicts which Region the trajectory eventually lies in.

The fast i_L term for Region II for small L and large ω is

$$I_o - \frac{v'_C + A \sin(\omega t')}{R_2}. \quad (3.4)$$

Define $g(t') := I_o R_2 - A \sin(\omega t')$. If $v'_C = g(t')$, the fast i_L term is zero; if $v'_C > g(t')$, the fast i_L term is positive; if $v'_C < g(t')$, the fast i_L term is negative. Hence $g(t')$ acts as a time-controlled gate. It allows certain trajectories to pass through to Region III while the others are returned to Region I. Picture $g(t')$ as the lower end of a wall lying on the line $i_L = I_o$. The wall oscillates vertically with amplitude A and frequency ω and the oscillation is centered at the break in the resistor characteristic. Any trajectory which leaves Region I below this oscillating barrier will pass into Region III. Trajectories hitting the barrier will pass through it into Region II, turn, and reenter Region I. From symmetry a similar gate exists at the other break in the resistor characteristic. See Figure 5.

We should mention here that $g(t')$ predicts whether the *long term* motion (when Region II is extended to the whole plane) is to the left or the right. This is not exactly what we want. We are interested in the *first* Region the trajectory enters after entering Region II. The two answers may not agree⁴. In Appendix III we show that an exact gate function does exist (without assumptions on L and ω) and is close to $g(t')$ for L small and ω large. For the purposes of our explanation the discrepancy between $g(t')$ and the actual gate function is unimportant.

⁴This will happen at the Region I/II boundary when the fast i_L term is small and negative. The slow i_L term (which is always positive) would then push the trajectory into Region I before the contribution from the fast i_L term grows enough to force the trajectory into Region III.

3.6. Overall Dynamics

We now turn our attention to the problem of subharmonics. To classify them we use rotation numbers. We define the rotation number of a periodic solution as two positive integers separated by a slash, $\rho := p/q$, where p is the number of times the origin is encircled by the periodic solution⁵ and q , called the order of the subharmonic, is the number of periods of the forcing term contained in one period of the periodic solution. This concept of rotation number is less general than the usual one since it can only be applied to a periodic solution. Yet, in an experimental situation, it is much more useful since it corresponds to the method actually used to measure rotation numbers. It also conveys more information. A rotation number of $2/3$ is distinct from a rotation number of $4/6$. For a discussion on the exact relationship between the two concepts of rotation number, see **Appendix IV**.

Plots of rotation numbers for various regions of ϵ and b are given in Figure 6. These plots are similar to those in [4] except we have plotted data only at the exact points of the b - ϵ plane for which we ran a simulation. Most of the remaining Figures are various collections of periodic solutions. They will be discussed later, but it may be helpful to glance at them now. For details on how these results were obtained see **Appendix I**. We used ϵ , b and T (dimensionless period $:= 2\pi/\omega'$) as parameters so the results can be easily compared to previous authors' work. Use equations (1.4) to change back to circuit parameters. All results in this paper were computed with $R_1 = -R_2 = R_3 = 1\Omega$, $I_o = 1A$, and $\omega' = 1$.

3.6.1. Numerical Verification of Some of Levi's Results

Levi studied the dimensionless relaxation oscillation equation for ϵ small. We have seen the dynamics for small ϵ are simple so we will begin our discussion with this case. Unless explicitly stated otherwise, this section deals exclusively with the case of small ϵ . Remember that small ϵ implies large ω since Levi holds ω' constant. We will not attempt to prove the existence of subharmonics, but will be satisfied explaining some of their properties.

Figure 7 is two plots of $1/\rho$ versus b . Figure 7(a) fixes ϵ at 0.005. It may be hard to tell from the Figure, but every *odd* order subharmonic from $\rho = 1/1$ to $\rho = 1/69$ is present and none other. Figure 8 shows some representative periodic solutions for $\epsilon = 0.005$.

⁵All trajectories encircle the origin counterclockwise for the equation studied here.

Figure 7(b) is a plot of $1/\rho$ versus b for $\epsilon=0.0025$. The triangles on the b axis indicate values of b for which the program did not converge in the allowed time. The value of ϵ for Figure 7(b) is half that of Figure 7(a). Thus to keep dimensionless frequency for each Figure constant at $\omega'=1$, we need to double the dimensioned frequency ω . Since the slow eigenvalue (which governs the decay along the resistor characteristic) is independent of ϵ for ϵ small, the doubling of ω allows twice as many oscillations to fit in the same length of resistor characteristic. This explains the doubling of the range of the $1/\rho$ axis in Figure 7(b).

The preponderance of odd order subharmonics for small ϵ is easily explained by the gate mechanism. Consider a trajectory oscillating down the resistor characteristic in Region I (Figure 9). The gate is oscillating at the same frequency. When i_L is at a minimum in its oscillations, the gate is at a maximum. From geometrical considerations i_L will tend to first hit the boundary near one of its minima. This is a time when the gate is at its highest point. The same argument applies when the trajectory passes from Region III to Region II except that there i_L first hits the boundary near a maximum. Since one boundary is crossed near a minimum and the other near a maximum, the number of half periods (of the forcing term) between the two times must be odd: $(2k+1)T/2$ for some positive integer k . The total period of the subharmonic is simply twice that⁶ or $(2k+1)T$ which is an odd multiple of the forcing period.

The observation that i_L first hits the boundary near a minimum seems obvious enough, but it fails for small A . Consider the trajectory in Region I. Note that the horizontal motion of the trajectory has two components: the decay of the slow eigenvector toward the left and the oscillation of i_L alternately to the left and to the right. For large A the rightward oscillation of i_L overwhelms the leftward motion of the slow eigenvector and for nearly half a period the horizontal motion is to the right away from the boundary. However, if A is small enough, the leftward motion of the slow eigenvector will be larger than the rightward motion of the i_L oscillation, there will be no net rightward motion and the boundary may be crossed at any point in the oscillation. Thus *even* order subharmonics might be found for small A . In fact, we did find a $1/70$ subharmonic for $\epsilon=0.005$ and $b=0.007$. Levi's A and B intervals are guaranteed to exist inside an interval of b equal to $[\bar{c}, 1-\bar{c}/2]$ where $\bar{c} > 0$ is some small constant. Hence for $\epsilon=0.005$, $\bar{c} > 0.007$.

⁶To be completely honest we note that this step depends on k being the same for Regions I and III. This may be proven using symmetry arguments. An intuitive explanation is that the trajectory must travel the same distance down the resistor characteristic in Region I as it travels up the resistor characteristic in Region III. Therefore the times spent in each Region cannot differ by a whole period.

For larger ϵ the problem becomes more complex. An examination of the fast i_L term of the exact solution shows the gate is still sinusoidal, but it is no longer 180° out of phase with the i_L oscillations. Figure 10 shows two portions of a periodic solution, each one entering Region II from Region I. One of them hits the gate and reenters Region I while the other passes below the gate and enters Region III. None of the small ϵ trajectories we saw ever hit the gate, they always passed below it.

Returning to the small ϵ discussion and Figure 7(a), notice that as b decreases from 1.1 the interval of existence of each subharmonic shrinks. The result is that a smooth curve joining the centers of each row of triangles is not a straight line, but is slightly bent. This bowing can be explained by the time-controlled gate. The amplitude of oscillation of the gate is b (for $\omega' = 1$, $A = b$). Thus for large b , the gate opens wider than for small b . In fact, for $b \geq 1$ the gate crosses the i_L axis. This is where the 1/1 subharmonic exists. As b decreases, the amplitude of the gate oscillation decreases and the trajectory must travel farther down the resistor characteristic to pass under the barrier (Figure 8). The decrease in the "width" of the gate is proportional to b which is why Figure 7 is nearly linear. The bowing results from the previously remarked bunching of the trajectories as they travel down the resistor characteristic.

3.6.1.1. The Window Map

We now turn our attention away from trajectories and toward the Poincaré map. The Poincaré map, $P: \mathbf{R}^2 \rightarrow \mathbf{R}^2$, takes the point (i_{Lo}, v_{Co}) to the point $(i_L(T), v_C(T))$ where the trajectory has initial conditions $(i_L(0), v_C(0)) = (i_{Lo}, v_{Co})$ and T is the period of the forcing term. Thus P maps a point to where it will be one period later. The Poincaré map is useful for it turns a three-dimensional problem into a two-dimensional one.

The key construction in Levi's proof is the window map, N . N takes a point from a skinny rectangle r in the $i_L - v_C$ plane to a point in the symmetrically located rectangle $-r$ (Figure 11(a)). The rectangle r is chosen such that it is one Poincaré map long, that is, the segment AA' is mapped into the segment BB' under one iteration of P .

The window map is constructed from the Poincaré map as follows. Consider the image of r after one Poincaré iteration (Figure 11(b)). Levi shows that the bottom part of r is swept over into Region III with no change in orientation. The top portion of r is shifted downward, but remains in Region I. A very small length

of r is stretched across Region II and joins the two major portions.

One more iteration of P causes the whole image $P^2(r)$ to lie in Region III and after some more Poincaré iterations the image of r has reached the vicinity of $-r$ (Figure 11(c)) and we have the window map N^7 . $N(r)$ consists of three parts: the stretched region and the two undistorted regions which the stretched region connects. The stretched portion corresponds to the very small slice of the original set r which is the unmarked area in Figure 11(d).

There are two things to note here. The window map N contains a snake-like bend. This bend gives rise to a Smale's Horseshoe and chaotic behavior. Also, Levi showed that the lengths of the two undistorted portions of r (the dotted and cross-hatched areas in Figure 11(d)) change with the amplitude of the forcing term. This dependence explains the patterns in the behavior of the equation as the amplitude is varied.

Figure 12 is a computer simulation of this phenomenon. Levi proves r is so skinny that it can be accurately approximated by a line segment. In Figure 12(a) the line segment is chosen such that the top endpoint is mapped into the bottom endpoint under one iteration of the Poincaré map. Figure 12(b) shows the segment after one application of P , Figure 12(c) after one more application. Figure 12(d) shows $P^2(r)$ for a slightly different forcing amplitude. Notice the change in lengths of the two segments of $P^2(r)$. These Figures were obtained by dividing the initial segment into one hundred evenly spaced points. At this resolution, the stretched connecting piece does not show. We increased the resolution to the equivalent of one hundred thousand evenly spaced points along the segment and the stretched piece still did not show which gives some idea of how small a portion of r it actually is.

3.6.2. More on Single Loop Subharmonics

Now we expand our discussion and consider the behavior of the system for large ϵ . Figure 13 is a collection of single loop subharmonics of order one to six for larger values of ϵ . Note the periodic solutions tend to be fatter. This is mainly due to the dependence of ω on ϵ . The most striking feature is the existence of even order subharmonics. As expected, the $1/6$ subharmonic exists for small b , but the $1/4$ subharmonic can occur for $b > 0.3$ and the $1/2$ subharmonic exists for $b > 0.7$. This does not contradict our earlier prediction that even order subharmonics should only occur for small amplitudes since ϵ is well out of the range in which the

⁷It is not this easy, but the basic idea is still valid. See [2] for the details.

prediction is valid.

Next note the similarity in shape between the left half of the $1/2$ subharmonic and the left half of the $1/3$ subharmonic. Also note the similarity between the right halves of the $1/2$ and $1/1$ subharmonics. It appears that for $i_L > 0$ the trajectory behaves like a $1/1$ subharmonic and when Region III is entered it behaves like a $1/3$ subharmonic. Moreover, $0.5 (1/1) + 0.5 (1/3) = 1/2$ ⁸. So in some sense a $1/2$ subharmonic is made up of half a $1/1$ subharmonic and half a $1/3$ subharmonic. The fact that the $\rho = 1/2$ region of existence on the $b-\epsilon$ plane (see Figure 6) lies between the $\rho = 1/1$ and $\rho = 1/3$ regions lends weight to this interpretation.

The same observation can be made for $\rho = 1/4$ where the left half looks like $\rho = 1/5$ and the right half like $\rho = 1/3$. Again $0.5 (1/3) + 0.5 (1/5) = 1/4$ and the $\rho = 1/4$ region lies between the $\rho = 1/3$ and $\rho = 1/5$ regions. A similar argument holds for $\rho = 1/6$.

It appears the even order, single loop subharmonics are built from the odd order, single loop subharmonics. Picture it as follows: For a $1/1$ subharmonic the oscillations of the trajectory somehow becomes synchronized to the oscillation of the gates. The trajectory eventually settles down and follows a closed path. This periodical solution is symmetrical about the origin; that is the trajectory behaves the same when it enters Region I as when it enters Region III. Similarly a $1/3$ subharmonic becomes synchronized to the gates except it spends an extra period in each of Regions I and III. For parameter values between the ones that yield $1/1$ and $1/3$ subharmonics, a mixture of the two types of behavior occurs. When the trajectory enters Region I its initial conditions there make it behave like a $1/1$ subharmonic. When it crosses to Region III its initial conditions there force it to spend an extra period in Region III in order to get past the gate and in this Region it behaves like a $1/3$ subharmonic. Somehow the two different types of behavior are linked by Region II and a stable subharmonic occurs. This description will become clearer as more examples are given.

3.6.3. Subharmonics With More Than One Loop

Figure 14(a) shows a $2/3$ subharmonic. It is clearly a combination of a full $1/1$ and a full $1/2$ subharmonic. Indeed, $1/1 + 1/2 = 2/3$. Again we see a mixture of single loop subharmonics. It is as if the solution would like to be $1/1$, but it cannot quite reach Region II to close the loop before the i_L oscillation swings the other way. It is forced to act like a $1/2$ subharmonic to get past the gate and cross to Region I. Note that the

⁸Rotation number arithmetic follows these laws: $r(p/q) = rp/rq$ and $p/q + r/s = (p+r)/(q+s)$.

$\rho = 2/3$ region is located between the $\rho = 1/1$ and $\rho = 1/2$ regions.

Figure 14(b) is a $3/5$ subharmonic. It consists of one $1/1$ subharmonic and two $1/2$ subharmonics. Note that $1/1 + 2(1/2) = 3/5$ and that the $\rho = 3/5$ region is located between the $\rho = 1/1$ and the $\rho = 1/2$ regions.

Figure 14(c) is interesting. It is a $13/15$ subharmonic made of eleven $1/1$'s and two $1/2$'s. As the plot was being produced, $1/1$ loops followed one after the other, each one in a slightly different position. Then, as the differences added up, the trajectory could not make it through the gate and did a $1/2$ loop followed by more $1/1$ loops, each one slightly out of phase with the previous one until it did another $1/2$ loop and closed in on itself.

All the periodic solutions we computed between the $1/1$ and $1/2$ regions could be similarly dissected. Always $n_1(1/1) = n_2(1/2) = p/q$ where n_1 and n_2 are the number of $1/1$ and $1/2$ subharmonics forming the p/q subharmonic. Also if $n_1 > n_2$, the region of existence of the subharmonic is nearer to the $1/1$ region than the $1/2$ region and vice versa.

If n_1 and n_2 are large, we expect the region of existence of the subharmonic to be smaller since a slight perturbation would ruin the delicate balance Region II provides between the different types of behavior. An examination of Figure 6 confirms this expectation.

Figure 15 shows some periodic solutions for parameters between the $1/2$ and $1/3$ regions. Again every subharmonic we found in this region could be split into $\rho = 1/2$ and $\rho = 1/3$ components. Again $n_2(1/2) + n_3(1/3) = p/q$.

In fact, every periodic solution we found was a combination of the two nearest single loop subharmonics. The single loop subharmonics are the building blocks of the multi-loop subharmonics and the even order, single loop subharmonics can be built from the odd order, single loop subharmonics. Thus the odd order, single loop subharmonics are the fundamental subharmonics of the forced relaxation oscillator.

There is some predictive power here. Suppose we want to know something about a $13/23$ subharmonic. Since $1/2 < 13/23 < 1$ we know the subharmonic is composed of $1/1$ and $1/2$ subharmonics. Solving $n_1(1/1) + n_2(1/2) = 13/23$ we get $n_1 = 3$ and $n_2 = 10$. Therefore, if it exists (and in this case it does), it is composed of three $1/1$'s and ten $1/2$'s and its region of existence is closer to the $1/2$ region than the $1/1$ region. We do not know beforehand in what order the component subharmonics occur. It may be that there

exists two subharmonics of equal rotation number, but differing sequences of component subharmonics.

This concept of the order in which component subharmonics occur helps explain random behavior in the relaxation oscillator. For ϵ small and b chosen in a B-type interval, Levinson showed that given *any* (perhaps nonperiodic) sequence of component subharmonics, there exists a trajectory which follows that sequence. Unfortunately, the set of initial points for all such random trajectories has measure zero and all observable trajectories tend to one of the two stable periodic solutions.

4. Summary and Conjecture

The main advantage of using piecewise linear analysis is the high accuracy in our numerical results. Another advantage is the concentration of all interesting behavior at the boundaries between Regions. This allowed us to introduce a gate function along each boundary which helped us explain some of the relaxation oscillation phenomena.

Study of the numerical results led us to the conclusion that all subharmonics are built from the nearest single loop subharmonics and that even order, single loop subharmonics are built from odd order, single loop subharmonics. The idea of a periodic solution becoming synchronized to the gates helped explain this behavior. An analytical explanation of the structure we have found is needed.

All our evidence supports the hypothesis that given $\rho = p/q$, with $p \leq q$ relatively prime and q odd, there exists a region of ϵ and b such that a p/q subharmonic exists. Since all observations occupy a finite time, arbitrarily large q implies the existence of essentially random behavior. Of course for q large the region of existence becomes quite small and may be hard to locate numerically. We did find a subharmonic with $\rho = 10/16$, but it was the only one with a common factor in p and q . It may be that any subharmonic exists with rotation number equal to $m(1/k) + n(1/(k+1))$ where m and n are arbitrary positive integers. Perhaps the odd order, relatively prime subharmonics have larger regions of existence than the others and are all that we could observe at our resolution. Again only an analytical explanation of the relaxation oscillation phenomena can answer these questions.

Acknowledgements

We would like to thank Dr. Michael Odyniec for his insightful comments and kind assistance in the preparation of this paper.

References

- [1] N. Levinson, "A second order differential equation with singular solutions," *Ann. Math.*, vol. 50, no. 1, 1949, pp. 127-153.
- [2] M. Levi, "Qualitative analysis of the periodically forced relaxation oscillations," *Mem. of Am. Math. Soc.*, vol. 32, no. 244, July 1981.
- [3] A. Andronov, A. Vitt, S. Khaikin, *Theory of Oscillators*, Addison-Wesley, New York, 1966.
- [4] J. Flaherty, F. Hoppensteadt, "Frequency Entrainment of a Forced van der Pol Oscillator," *Studies in Applied Math.*, vol. 58, 5-15, 1978.

Appendix I. The Computer Program

AI.1. The Program

To calculate the rotation numbers the program samples the trajectory once every input period. That is, it calculates $i_L(t_0 + kT)$ and $v_C(t_0 + kT)$ where k is a positive integer and T is the input period. These points correspond to iterations of the Poincaré map. If the solution is an n th order subharmonic, these points will be periodic with period n .

The program computes which Region the initial condition is in and then searches for the first time t_1 that the trajectory leaves that Region. The program then calculates any points of the Poincaré map which lie between t_0 and t_1 . Each time a new point of the Poincaré map is calculated, it is compared to all previously computed points to test for convergence to a periodic solution. If convergence is found, the program stops; if not, the point at t_1 is taken as a new initial condition in a new Region and the process is repeated. In any case the program never computes more than 500 Poincaré iterations.

AI.2. The Boundary Search

The simplest way to find the boundary crossing is to calculate points on the trajectory every Δt seconds where Δt is some small time step. Suppose the first such point which lies in a new Region occurs at time $t_0 + k\Delta t$. Then the boundary crossing must occur within the interval $(t_0 + (k-1)\Delta t, t_0 + k\Delta t)$. Now the computer can halve the time interval and zero in on the boundary crossing with the desired degree of accuracy. We call this the small step method.

The program uses this method in Region II and a variation of it in Regions I and III. A portion of a typical trajectory is shown in Figure I.1. To find t_1 it is unnecessary to start a small step search at t_0 . What the program does is calculate the points on the trajectory occurring at the local minima of i_L . When one of these minima is in a new Region, the program backs up to the previous minimum and begins a small step search there. Thus only the crosshatched part of the trajectory is searched. It should be pointed out that a closed form analytical expression is available to calculate the locations of the i_L minima.

AI.3. Accuracy

There are two main places where errors occur. One is the boundary crossing and the other is the convergence test on the Poincaré iterations.

In calculating the boundary crossing, we required $|i_L - I_0| < 10^{-10}$. For the Poincaré convergence, we required

$$|i_L(nT) - i_L(kT)| + |v_C(nT) - v_C(kT)| < 10^{-10}. \quad (\text{I.1})$$

When (I.1) was satisfied, we concluded that the solution was an $(n-k)$ th order subharmonic. We used 64 bit floating point representation for all noninteger variables.

AI.4. The Data

To get the plots of ρ -vs- ϵ we divided the b - ϵ plane into evenly spaced rows. Simulations were run at evenly spaced points along each row. Two computer runs were performed for each row: one starting with the minimum b value and incrementing it, the other starting with the maximum b value and decrementing it. The initial condition for each simulation was the final point calculated in the previous simulation. Thus each (b, ϵ)

point was simulated from two “directions”. This allowed us to locate (b, ϵ) points with two rotation numbers (hysteresis).

Appendix II. Derivation of Small L and Large ω Approximations

In this Appendix we derive equations (2.2), (3.2) and (3.3) for Region I. The derivation for Region III is identical. The derivation for Region II is slightly different since $R_2 < 0$, but the results are the same.

AII.1. Approximations for Small L

AII.1.1. The Autonomous Contribution

In Region I, rewrite the eigenvalues as

$$s_{11} = -\frac{R_1}{2L} + \left\{ \left(\frac{R_1}{2L} \right)^2 - \frac{1}{LC} \right\}^{\frac{1}{2}} = -\frac{R_1}{2L} \left[1 - \left(1 - \frac{4L}{R_1^2 C} \right)^{\frac{1}{2}} \right]. \quad (\text{AII.1})$$

For L small, approximate the square root using the first two terms of the Binomial Expansion to get

$$s_{11} \approx -\frac{R_1}{2L} \left[1 - \left(1 - \frac{2L}{R_1^2 C} \right) \right] = -\frac{1}{R_1 C}. \quad (\text{AII.2})$$

Similarly for s_{21} :

$$\begin{aligned} s_{21} &= -\frac{R_1}{2L} - \left\{ \left(\frac{R_1}{2L} \right)^2 - \frac{1}{LC} \right\}^{\frac{1}{2}} = -\frac{R_1}{2L} \left[1 + \left(1 - \frac{4L}{R_1^2 C} \right)^{\frac{1}{2}} \right] \\ &\approx -\frac{R_1}{2L} \left[1 + \left(1 - \frac{2L}{R_1^2 C} \right) \right] = -\frac{R_1}{2L} \left[2 - \frac{4L}{R_1^2 C} \right] \\ &\approx -\frac{R_1}{L} \end{aligned} \quad (\text{AII.3})$$

where we have ignored the term proportional to L with respect to 2.

Now that we have the eigenvalues, we approximate the eigenvectors. For the autonomous case the first eigenvector is

$$v_{11} = \frac{i_L(t_0) + s_{21}C(v_C(t_0) - V_{o1})}{s_{11} - s_{21}} \begin{bmatrix} s_{11} \\ -1/C \end{bmatrix}. \quad (\text{AII.4})$$

Since $s_{21} \gg s_{11}$, the denominator becomes $-s_{21}$ and

$$\begin{aligned} v_{11} &\approx \left\{ \frac{i_L(t_0)}{s_{21}} + C(v_C(t_0) - V_{o1}) \right\} \begin{bmatrix} -s_{11} \\ 1/C \end{bmatrix} \\ &\approx \left\{ -\frac{Li_L(t_0)}{R_1} + C(v_C(t_0) - V_{o1}) \right\} \begin{bmatrix} R_1/L \\ 1/C \end{bmatrix} = \begin{bmatrix} \frac{Li_L(t_0)}{R_1^2 C} + \frac{v_C(t_0) - V_{o1}}{R_1} \\ \frac{Li_L(t_0)}{R_1 C} + v_C(t_0) - V_{o1} \end{bmatrix} \\ &\approx \begin{bmatrix} \frac{v_C(t_0) - V_{o1}}{R_1} \\ v_C(t_0) - V_{o1} \end{bmatrix} \end{aligned} \quad (\text{AII.5})$$

where we have ignored the term proportional to L since it is small compared to the $v_C(t_0)$ term.

The second eigenvector in Region I for the autonomous case is

$$\begin{aligned} v_{2i} &= \frac{i_L(t_0) + s_{1i}C(v_C(t_0) - V_{o1})}{s_{1i} - s_{2i}} \begin{bmatrix} -s_{2i} \\ 1/C \end{bmatrix} \\ &\approx \left\{ \frac{i_L(t_0) + s_{1i}C(v_C(t_0) - V_{o1})}{s_{2i}} \right\} \begin{bmatrix} s_{2i} \\ -1/C \end{bmatrix} \\ &\approx \frac{L}{R_1} \left\{ i_L(t_0) - \frac{(v_C(t_0) - V_{o1})}{R_1} \right\} \begin{bmatrix} R_1/L \\ 1/C \end{bmatrix} \\ &\approx \begin{bmatrix} i_L(t_0) - \frac{v_C(t_0) - V_{o1}}{R_1} \\ 0 \end{bmatrix} \end{aligned} \quad (\text{AII.6})$$

where we have completely ignored the v_C component since it is proportional to L . This approximation may seem unwarranted, but if it is considered in terms of the magnitude and angle of the eigenvector, it is valid.

AII.1.2. The Nonautonomous Contribution

For convenience we consider the i_L and v_C terms separately.

AII.1.2.1. The i_L Coefficients

The i_L coefficient for the s_{11} exponential is

$$\begin{aligned} & \frac{As_{11}\cos(\omega t_o + \phi_{11})}{(s_{11} - s_{21})L\sqrt{s_{11}^2 + \omega^2}} \\ & \approx -\frac{As_{11}\cos(\omega t_o + \phi_{11})}{s_{21}L\sqrt{s_{11}^2 + \omega^2}} = -\frac{A\cos(\omega t_o + \phi_{11})}{R_1\sqrt{1 + (\omega R_1 C)^2}}. \end{aligned} \quad (\text{AII.7})$$

where

$$\phi_{11} = \text{Tan}^{-1} \frac{s_{11}}{\omega} \approx \text{Tan}^{-1} \frac{1}{\omega R_1 C}. \quad (\text{AII.8})$$

The i_L coefficient for the s_{12} exponential is

$$\begin{aligned} & -\frac{As_{21}\cos(\omega t_o + \phi_{21})}{(s_{11} - s_{21})L\sqrt{s_{21}^2 + \omega^2}} \\ & \approx \frac{A\cos(\omega t_o + \phi_{21})}{L\sqrt{s_{11}^2 + \omega^2}} = \frac{A\cos(\omega t_o + \phi_{21})}{R_1\sqrt{1 + (\omega L/R_1)^2}} \\ & \approx -\frac{A}{R_1}\sin(\omega t_o) \end{aligned} \quad (\text{AII.9})$$

where ϕ_{21} has been approximated by

$$\phi_{21} = \text{Tan}^{-1}(s_{21}/\omega) \approx \text{Tan}^{-1}(R_1/\omega L) \approx \text{Tan}^{-1}(\infty) = \pi/2. \quad (\text{AII.10})$$

The sinusoidal term for i_L is

$$\begin{aligned} & \frac{A\omega\sin(\omega t + \theta_1)}{L\sqrt{(s_{1i}^2 + \omega^2)(s_{2i}^2 + \omega^2)}} \\ & \approx \frac{A\omega\sin(\omega t + \theta_1)}{L\sqrt{((-1/R_1 C)^2 + \omega^2)((-R_1/L)^2 + \omega^2)}} \\ & \approx \frac{A\omega\sin(\omega t + \theta_1)}{L\sqrt{((-1/R_1 C)^2 + \omega^2)(-R_1/L)^2}} = \frac{A\omega C\sin(\omega t + \theta_1)}{\sqrt{1 + (\omega R_1 C)^2}} \end{aligned} \quad (\text{AII.11})$$

where

$$\begin{aligned} \theta_1 & = \arg(-2\alpha_1\omega + j(\omega_o^2 - \omega^2)) = \arg(\omega R_1/L + j(1/LC - \omega^2)) \\ & \approx \arg(\omega R_1/L + j(1/LC)) = \arg(\omega R_1 C + j). \end{aligned} \quad (\text{AII.12})$$

AII.1.2.2. The v_C Terms

To make things simple, note that the nonautonomous contribution to the v_C s_{11} exponential is just the i_L contribution multiplied by

$$-\frac{\omega_o^2 L}{s_{11}} \approx R_1. \quad (\text{AII.13})$$

Similarly the nonautonomous contribution to the s_{21} exponential of v_C is the contribution to the s_{21} exponential

of i_L multiplied by

$$- \frac{\omega_o^2 L}{s_{21}} \approx \frac{L}{R_1 C}. \quad (\text{AII.14})$$

Multiplying the appropriate i_L terms and ignoring terms proportional to L yields the desired approximations. Since the coefficient of the s_{21} exponential of v_C is proportional to L we approximate it by zero.

To get the approximation for the steady state v_C term, take the i_L steady state term, switch the sine to cosine and multiply by a factor of $1/\omega C$.

AII.2. Approximations for Small L and Large ω

Remember that Levi holds dimensionless frequency ω' constant during his analysis. The relationship between dimensioned frequency ω and dimensionless frequency is

$$\omega = \omega' \omega_o = \frac{\omega'}{\sqrt{LC}}. \quad (\text{AII.15})$$

We set $\omega' = 1$ to get $\omega = \sqrt{LC}$. Therefore ω^2 is proportional to $1/L$. In making the small L approximations, we never ignored a term proportional to $1/L$ with respect to a term containing anything more than a proportionality to ω except when approximating θ_1 . Hence, except for θ_1 , we are justified in applying the large ω approximations directly to the results of Section AII.1 and we do not have to start from the exact equation (3.1).

AII.2.1. The i_L Coefficients

For ω large, equation (AII.7) becomes

$$- \frac{A \cos(\omega t_o + \phi_{11})}{\omega R_1^2 C} \approx 0. \quad (\text{AII.16})$$

For ω large equation (AII.9) is unchanged. Equation (AII.11) becomes

$$\begin{aligned} \frac{A \omega C \sin(\omega t + \theta_1)}{\omega R_1 C} &= \frac{A}{R_1} \sin(\omega t + \theta_1) \\ &\approx \frac{A}{R_1} \sin(\omega t). \end{aligned} \quad (\text{AII.17})$$

where we have used the definition of θ_1 and the fact that $\omega = \omega_o$ to get $\theta_1 = 0$.

AII.2.2. The v_C Terms

The nonautonomous contribution to the transient of v_C is zero as it was in the previous section. The magnitude of the steady state v_C term is the magnitude of the steady state i_L term multiplied by $1/\omega C$. It is, therefore, proportional to $1/\omega$ and is zero.

Appendix III. The Gate Function

AIII.1. Definitions

Consider a point in Region I. As time increases the point travels according to equation (1.6) and traces out a specific trajectory. The point will eventually hit the Region I/II boundary and enter Region II. The point must eventually leave Region II. It can do this in only two ways: it can either return to Region I in which case we call it a returning trajectory or it can pass into Region III in which case we call it a passing trajectory. These definitions are local in the sense that a trajectory can be a returning type at one boundary encounter and a passing type at the next. Let t_0 be the time when the trajectory hits the Region I/II boundary. Then $i_L(t_0) = I_0$. Define $v_{C_0} := v_C(t_0)$ to be the corresponding value of v_C at the boundary. The question is: Is there a function $\gamma(t_0)$ such that if $v_{C_0} < \gamma(t_0)$ then the trajectory passes to Region III while for $v_{C_0} > \gamma(t_0)$ the trajectory returns to Region I? We call $\gamma(t_0)$ a gate function.

AIII.2. Existence of the Gate Function

Let's examine the i_L solution for $t \geq t_0$ with initial conditions $i_L(t_0) = I_0$ and $v_C(t_0) = v_{C_0}$. Clearly for v_C large enough the trajectory enters Region I directly. It is also clear that for v_{C_0} negative enough, the trajectory will immediately cross Region II and enter Region III. Due to the continuous dependence of trajectories on initial conditions, as v_{C_0} is varied between these two extremes there must exist some value(s) of v_{C_0} at which the behavior of the trajectory changes from a returning type to a passing type.

To see how the trajectory changes with v_{C_0} , let's examine

$$\frac{\partial i_L}{\partial v_{C_0}} = \frac{s_{11}s_{22}C}{s_{12}-s_{22}} \left\{ e^{s_{12}(t-t_0)} - e^{s_{22}(t-t_0)} \right\}. \quad (\text{AIII.1})$$

$\frac{\partial i_L}{\partial v_{C_0}}$ is positive if the bracketed factor is positive. If $s_{12} > s_{22} > 0$, the bracketed factor is positive. Since

$s_{12} - s_{22} = \sqrt{\alpha_2^2 - \omega_0^2} > 0$ and the eigenvalues in Region II are positive, the bracketed factor is, in fact, positive and $i_L(t)$ is a strictly monotone increasing function of v_{C_0} . This fact plus the observations in the previous paragraph guarantee a unique point $\gamma(t_0)$ on the $i_L = I_0$ line such that trajectories with $v_{C_0} > \gamma(t_0)$ return to Region I while those with $v_{C_0} < \gamma(t_0)$ pass into Region III. This is the desired result. Due to continuity of trajectories with respect to initial conditions, $\gamma(t_0)$ is continuous in t_0 .

AIII.3. Approximations to the Gate Function

In this section we examine the fast and slow i_L terms and present an approximation for $\gamma(t_0)$ valid for small L and large ω .

AIII.3.1. The Slow Eigenvector

We are not interested in those trajectories which pass from Region II into Region I. That is we are only interested in v_{C_0} such that $\dot{i}_L(t_0) \leq 0$. From equation (1.6) this is the range

$$v_{C_0} \leq R_2 - A \sin(\omega t_0). \quad (\text{AIII.2})$$

The right hand side is simply a sinusoidal oscillation of amplitude A centered at the break in the resistor characteristic.

We now show that the slow i_L term is positive if $A \leq s_{12}L$. The slow i_L term is

$$\frac{1}{s_{12} - s_{22}L} \left\{ -s_{22}L I_0 - v_{C_0} + \frac{s_{22}A \cos(\omega t + \phi_{22})}{\sqrt{s_{22}^2 + \omega^2}} \right\}. \quad (\text{AIII.3})$$

To show the slow i_L term is positive requires showing the bracketed factor is positive. Since we are only interested in v_{C_0} values satisfying (AIII.2), we evaluate the bracketed factor in (AIII.3) with $v_C = R_2 I_0 - A \sin(\omega t_0)$. If this expression is positive, then it will be positive for any v_{C_0} satisfying (AIII.2).

The substitution yields

$$-s_{22}L I_0 - R_2 I_0 + A \sin(\omega t_0) - \frac{s_{22}A \cos(\omega t_0 + \phi_{22})}{\sqrt{s_{22}^2 + \omega^2}}. \quad (\text{AIII.4})$$

Combining the sinusoids (AIII.4) becomes

$$-(R_2 + s_{22}L) I_0 + \frac{\omega A}{\sqrt{s_{22}^2 + \omega^2}} \cos(\omega t_0 + \theta) \quad (\text{AIII.5})$$

where the exact value of θ is unimportant. (AIII.5) is a minimum when the cosine is equal to negative one:

$$-(R_2 + s_{22}L)I_o - \frac{\omega A}{\sqrt{s_{22}^2 + \omega^2}}. \quad (\text{AIII.6})$$

The term containing A is a minimum when $\omega = \infty$. This substitution yields $-(R_2 + s_{22}L)I_o - A$ which is positive when

$$A < -(R_2 + s_{22}L)I_o = s_{12}LI_o. \quad (\text{AIII.7})$$

Thus our claim is proved. To give the reader a feeling for (AIII.7), we note that $-R_2/2 < s_{12}L < -R_2$ for real s_{12} . For the rest of this Appendix we restrict our discussion to A satisfying (AIII.7).

AIII.3.2. The Fast Eigenvector

The fast i_L term is

$$\frac{s_{12}}{s_{12} - s_{22}} \left\{ I_o + \frac{1}{s_{12}L} v_{Co} + \frac{A \cos(\omega t_o + \phi_{12})}{L \sqrt{s_{12}^2 + \omega^2}} \right\}. \quad (\text{AIII.8})$$

It is negative when

$$v_{Co} < -s_{12}LI_o - \frac{s_{12}A \cos(\omega t_o + \phi_{12})}{\sqrt{s_{12}^2 + \omega^2}}. \quad (\text{AIII.9})$$

If v_{Co} satisfies (AIII.9) and if Region II is extended to the whole plane, then $i_L \rightarrow -\infty$ as $t \rightarrow \infty$. However we cannot conclude that the trajectory starting at such a v_{Co} does not reenter Region I before it enters Region III. What we can expect is that for small L and large ω , the difference between the right hand side of (AIII.9) and $\gamma(t_o)$ is small since by choosing L small enough the contribution from the fast i_L term may be made as large as we desire.

For small L and large ω (AIII.9) becomes

$$v_{Co} < I_o - A \sin(\omega t_o) =: g(t_o). \quad (\text{AIII.10})$$

To see $g(t_o)$ is very close to $\gamma(t_o)$, consider $i_L(t)$ for small L and large ω (equation (3.3)). It consists of a slow exponential, a fast exponential and a sinusoid. We consider three cases.

If the fast i_L term is zero, $v_{Co} = g(t_o)$, and the trajectory will return to Region I. This is true since the slow i_L term is positive.

If $v_{Co} < \gamma(t_o)$, the fast i_L term is negative enough to produce a large, rapid horizontal motion to the left which counteracts any rightward motion due to the slow exponential and/or the sinusoidal terms. In this case the trajectory passes to Region III.

The third case is a fast i_L term in between the two previous cases: $\gamma(t_0) < v_{C_0} < g(t_0)$. This range of v_{C_0} creates the difference between $\gamma(t_0)$ and $g(t_0)$ and correspond to a very small, negative fast i_L term. In this case the slow exponential term (and perhaps the sinusoidal term) pushes the trajectory back into Region I before enough time has elapsed for the fast exponential term to have any sizable effect. The fast eigenvalue is inversely proportional to L and is, therefore, very large. Thus the fast i_L term must be very small to account for the fact that the fast exponential has little initial effect on the trajectory. The result is that $g(t_0) - \gamma(t_0)$ is very small.

To see that $g(t_0)$ approaches $\gamma(t_0)$ as $L \rightarrow 0$, we note that both the slow exponential term and the sinusoidal term for $i_L(t)$ are independent of L for L small and ω large. The only dependence of $i_L(t)$ on L is through the fast eigenvalue, $s_{12} = -R/L$.

Let v_{C_0} satisfy $\gamma(t_0) < v_{C_0} < g(t_0)$ and let $L = L_0$. Let $t_1 > t_0$ be a time such that $i_{L_0}(t) \leq I_0$ for $t_0 < t < t_1$. Such a t_1 exists since the trajectory is initially pointing into Region II. If we decrease L the only change in $i_{L_0}(t)$ is in the fast exponential. Let $i_{L \text{ fast}}$ represent the absolute value of the fast i_L term. Then

$$-i_{L \text{ fast}} e^{\frac{-R_2(t_1-t_0)}{L_0}} \quad (\text{AIII.11})$$

is the fast exponential term for $i_{L_0}(t_1)$. Choose L_1 such that

$$i_{L \text{ fast}} e^{\frac{-R_2(t_1-t_0)}{L_1}} - i_{L \text{ fast}} e^{\frac{-R_2(t_1-t_0)}{L_0}} = 2I_0. \quad (\text{AIII.12})$$

Solve (AIII.12) for L_1 to get

$$L_1 = \frac{-R_2(t_1-t_0)}{\ln \left[\frac{2R_2 I_0}{v_{C_0}} + e^{\frac{-R_2(t_1-t_0)}{L_0}} \right]}. \quad (\text{AIII.13})$$

A simple check shows L_1 is well-defined and positive. With this new L_1 , $i_{L_1}(t_1) < -I_0$ and the trajectory passes to Region III. Hence by choosing L small enough, we can make $g(t_0) - \gamma(t_0)$ arbitrarily small.

Finally we note that $v_{C_0} < g(t_0)$ is simply (AIII.1). (AIII.1) gives those values of v_{C_0} for which the trajectory is passing from Region I into Region II. For L small, horizontal motion is very quick and the fact that the trajectory is moving to the left across the boundary predicts that the trajectory passes into Region III is no surprise.

Appendix IV. Rotation Numbers

We define the rotation number ρ of a periodic solution as two integers separated by a slash p/q . q is the number of periods of the forcing term in one period of the periodic solution and p is the number of times the projection of the periodic solution on the $t=0$ plane encircles the origin. This definition is directly applicable to experimental situations.

The usual definition of rotation number applies to a map of the plane into itself. Let P be such a map. Then the rotation number with respect to the origin for a point $z \neq 0$ is

$$\rho' := \lim_{n \rightarrow \infty} \frac{\arg(P^n z)}{2\pi n} \quad (\text{AIV.1})$$

where the $\arg(\cdot)$ function is a cumulative angle, not modulo 2π . We now show that a $\rho = p/q$ solution of a differential equation has $\rho' = \frac{p}{q}$ where ρ' is the rotation number of the Poincaré map of the differential equation.

To do this we need an assumption: The projection of the trajectory does not encircle the origin as t ranges from $(k-1)T$ to kT for any integer k satisfying $1 \leq k \leq q$ where T is the period of the driving function and q is the order of the subharmonic. This means that given $\mathbf{x}((k-1)T)$ and $\mathbf{x}(kT)$ (where \mathbf{x} is the state vector) we can determine the angle the projection of the trajectory subtends by calculating $\arg(\mathbf{x}(kT)) - \arg(\mathbf{x}((k-1)T))$. Without the assumption this expression would only be the angle modulo 2π (see Figure IV.1).

Suppose we have a periodic solution satisfying the assumption and with $\rho = p/q$. Let \mathbf{x} be a point on the solution at time $t=0$. Then

$$\begin{aligned} \rho' &= \lim_{n \rightarrow \infty} \frac{\arg(P^n \mathbf{x})}{2\pi q} \\ &= \lim_{l \rightarrow \infty} \frac{lq(\arg(P^q \mathbf{x}) - \arg(\mathbf{x})) + \arg(\mathbf{x})}{2\pi lq} \\ &= \frac{\arg(P^q \mathbf{x}) - \arg(\mathbf{x})}{2\pi q} \end{aligned} \quad (\text{AIV.2})$$

since the solution is periodic. Telescope the numerator to get

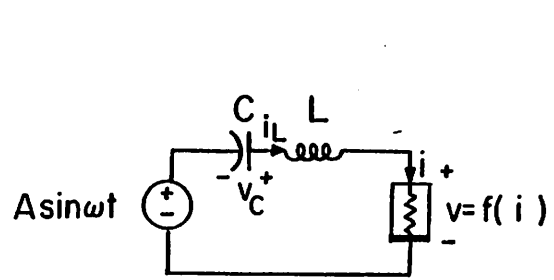
$$\rho' = \frac{(\arg(P^q \mathbf{x}) - \arg(P^{q-1} \mathbf{x})) + (\arg(P^{q-1} \mathbf{x}) - \arg(P^{q-2} \mathbf{x})) + \cdots + (\arg(P \mathbf{x}) - \arg(\mathbf{x}))}{2\pi q}$$

By the assumption, each parenthesized pair in the numerator is just the angle subtended by the projection of the trajectory during some period of the input. Therefore the numerator is equal to $2\pi p$ and our claim is

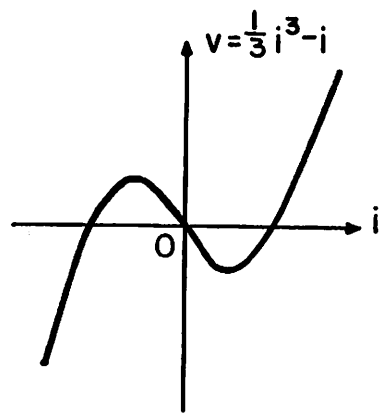
Figure Captions

- Figure 1 (a) the circuit governed by the relaxation oscillation equation;
(b) the van der Pol nonlinearity;
(c) the piecewise linear nonlinearity.
- Figure 2 (a) phase portrait for Region I extended to whole plane;
(b) phase portrait for Region II extended to whole plane;
(c) combined phase portrait for all three Regions.
- Figure 3 (a) limit cycle for the autonomous equation with $\epsilon = 0.005$;
(b) limit cycle for the autonomous equation with $\epsilon = 0.3$.
- Figure 4 portions of typical nonautonomous trajectories when (a) Region I and (b) Region III are extended to whole plane. Note the bunching of the trajectory as it travels along the resistor characteristic.
- Figure 5 different positions of the gates for different values of $\omega t'$.
- Figure 6 plots of rotation number ρ versus b and ϵ (labeled as eps). Each symbol represents a specific b, ϵ pair where actual results were obtained. A single number q indicates the order of a single loop subharmonic $\rho = 1/q$, two numbers separated by a hyphen $p-q$ indicate the rotation number of a multi-loop subharmonic $\rho = p/q$, @ indicates the program did not converge in the allotted time, in (a) two rotation numbers separated by a comma also indicate coexistence of rotation numbers, in (b) and (c) a capital letter indicates the existence of two different rotation numbers which are given at the bottom of the Figure. (b) is a more detailed view of the boxed region in (a) and (c) is a more detailed view of the boxed region in (b).
- Figure 7 (a) plot of $1/\rho$ versus b for $\epsilon = 0.005$;
(b) plot of $1/\rho$ versus b for $\epsilon = 0.0025$. Triangles lying on the b axis denote values of b for which the program did not converge in the allotted time.
- Figure 8 (a) $1/7$ subharmonic for $\epsilon = 0.005, b = 0.90$.
(b) $1/49$ subharmonic for $\epsilon = 0.005, b = 0.29$.
- Figure 9 relative positions of gate and trajectory: (a) gate at minimum and i_L at maximum;
(b) both gate and i_L at midpoint in oscillation;
(c) gate at maximum and i_L at minimum.
- Figure 10 a portion of a periodic solution for $\epsilon = 0.025$ and $b = 0.540$ which hits the gate and returns to Region I (solid) and a portion of the same periodic solution which passes under the gate and enters Region III (dashed).
- Figure 11 (a) positions of r and $-r$ (not drawn to scale);
(b) the image of r after one Poincaré iteration (not drawn to scale);
(c) the image of r after two Poincaré iterations and after enough Poincaré iterations (n) to get it in the vicinity of $-r$ (not drawn to scale);
(d) the three portions of r and their images under P^n .
- Figure 12 (a) line segment chosen for $\epsilon = 0.005$ and $b = 0.75$ such that point A maps to point C after one period of the forcing function;
(b) the line segment after one period of the forcing function (note that points B and B' are actually connected);
(c) the line segment after one more period.
(d) same as (c) but for $b = 0.78$.
- Figure 13 (a) $1/1$ subharmonic for $\epsilon = 0.12, b = 0.82$;
(b) $1/2$ subharmonic for $\epsilon = 0.15, b = 0.60$;
(c) $1/3$ subharmonic for $\epsilon = 0.10, b = 0.50$;
(d) $1/4$ subharmonic for $\epsilon = 0.09, b = 0.10$;
(e) $1/5$ subharmonic for $\epsilon = 0.07, b = 0.05$;
(f) $1/6$ subharmonic for $\epsilon = 0.06, b = 0.10$.

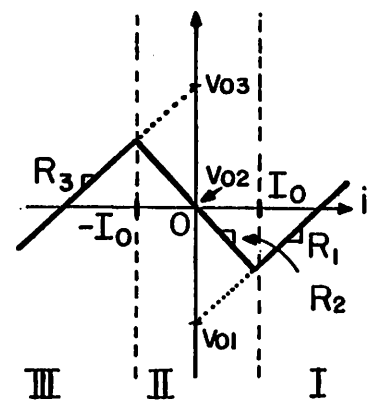
- Figure 14 (a) 2/3 subharmonic for $\epsilon = 0.165$, $b = 0.65$;
 (b) 3/5 subharmonic for $\epsilon = 0.155$, $b = 0.65$;
 (c) 13/15 subharmonic for $\epsilon = 0.19$, $b = 0.64$;
- Figure 15 (a) 2/5 subharmonic for $\epsilon = 0.17$, $b = 0.20$;
 (b) 4/9 subharmonic for $\epsilon = 0.1825$, $b = 0.28$;
- Figure I.1 to locate t_1 , the t' points are calculated. When t'_6 is found to lie in a new Region a small step search is initiated at t'_5 . The trajectory shown is for Region I extended to the whole plane.
- Figure IV.1 (a) a sample trajectory linking $\mathbf{x}((k-1)T)$ with $\mathbf{x}(kT)$ which satisfies the assumption;
 (b) a sample trajectory which does not satisfy the assumption.



(a)

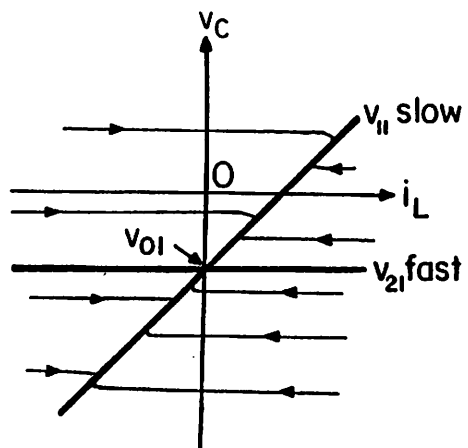


(b)

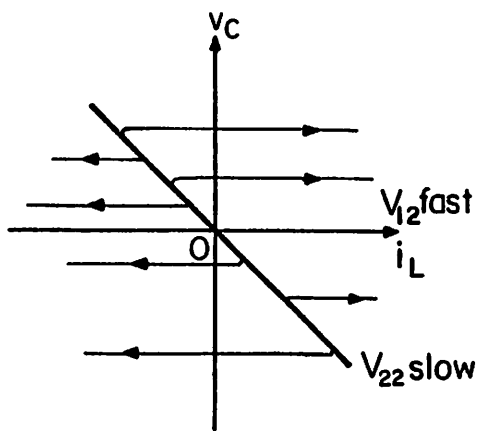


(c)

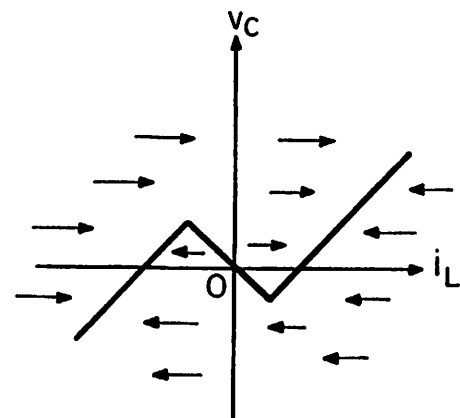
Fig. 1



(a)



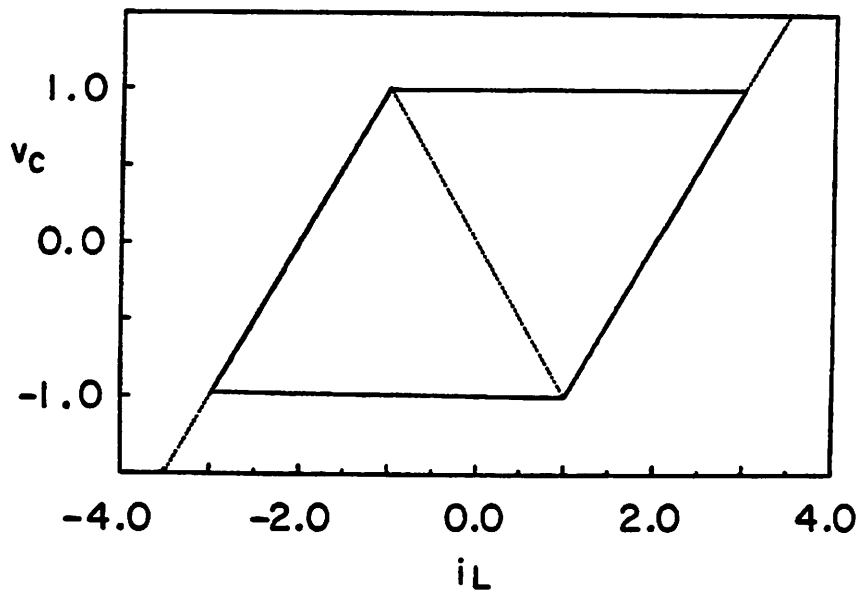
(b)



(c)

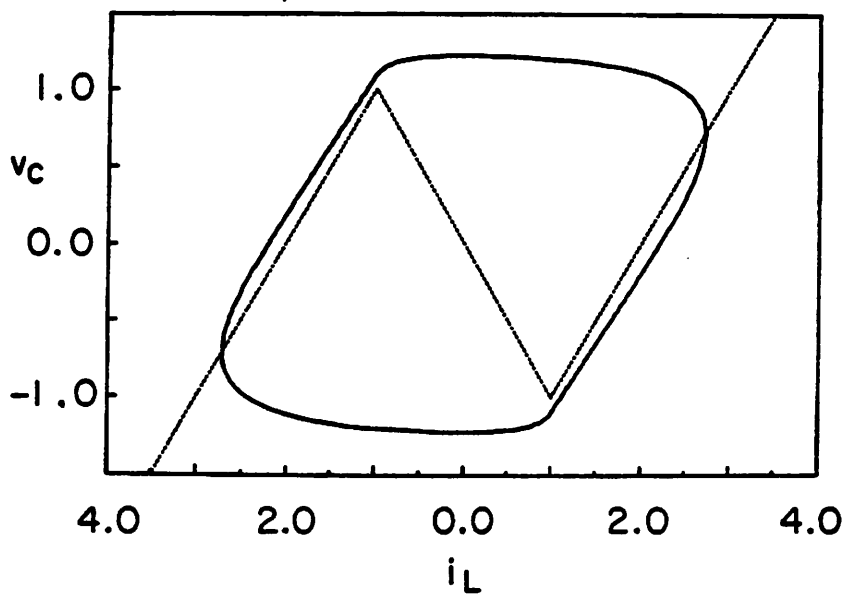
Fig. 2

$\text{eps}=0.005, b=0.0$



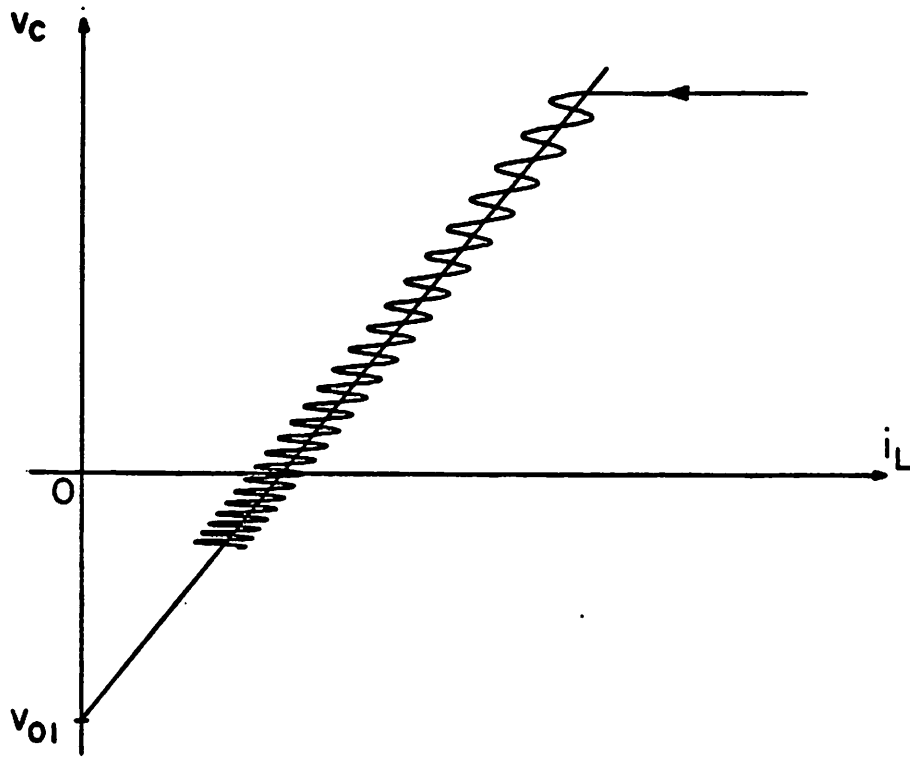
(a)

$\text{eps}=0.300, b=0.0$

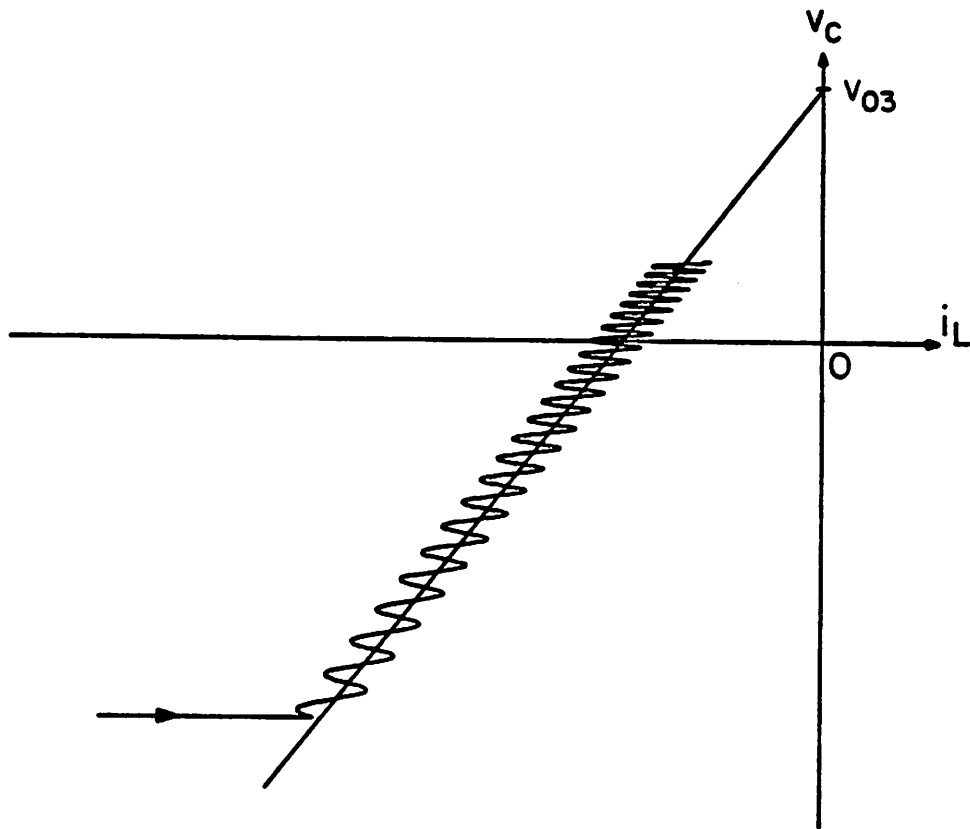


(b)

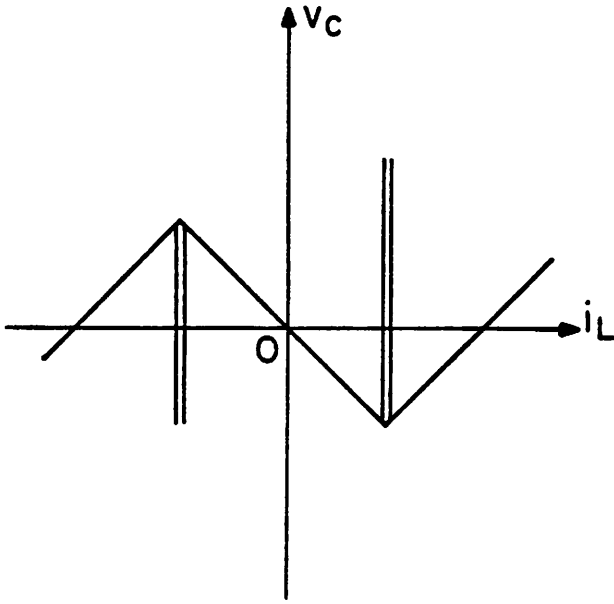
Fig. 3



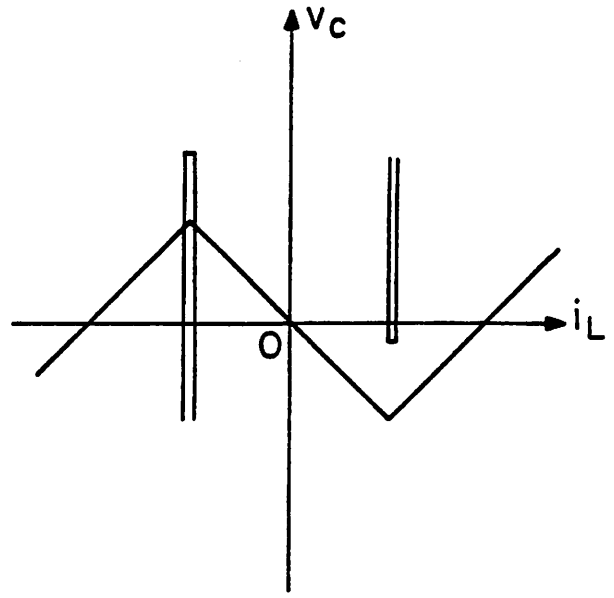
(a)



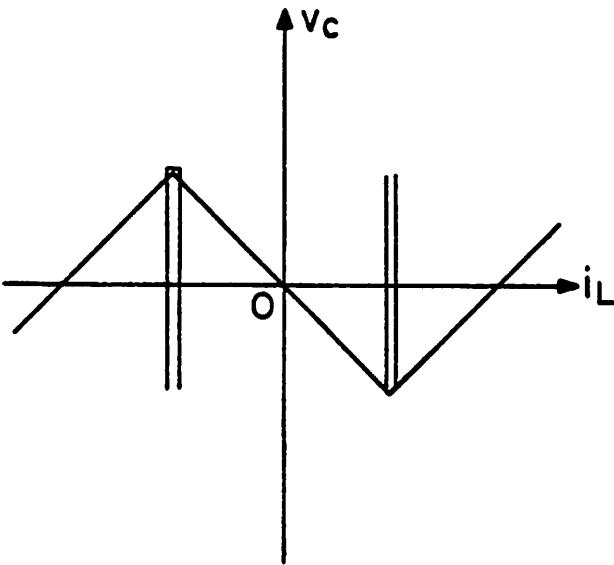
(b)
Fig. 4



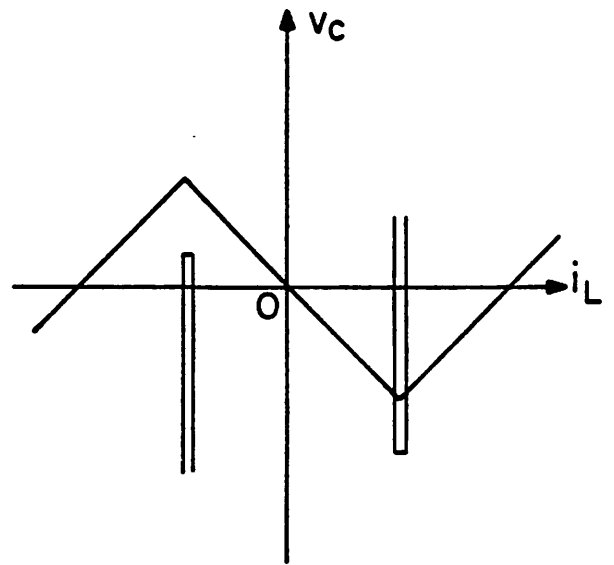
(a). $\omega t' = 0$



(b) $\omega t' = \pi/2$



(c) $\omega t' = \pi$



(d) $\omega t' = 3\pi/2$

Fig. 5

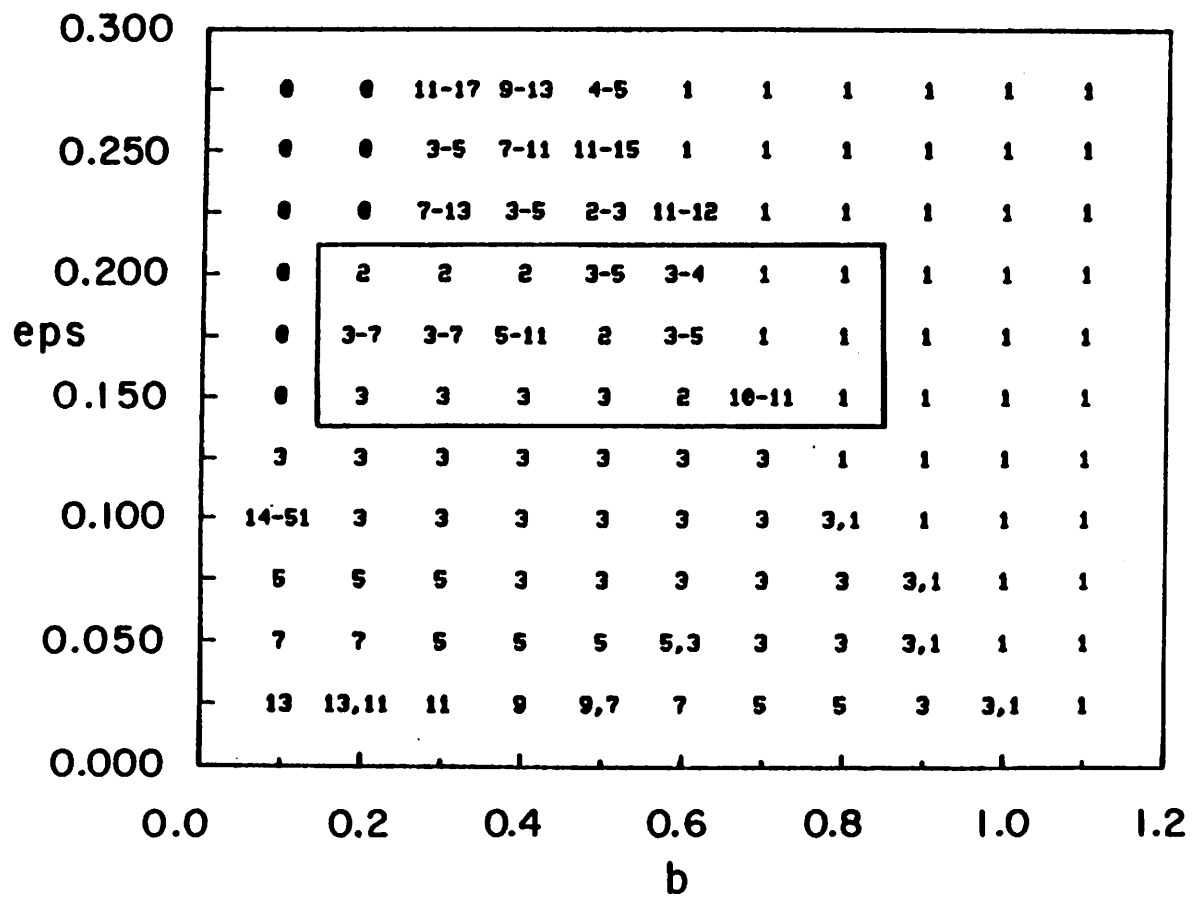


Fig. 6(a).

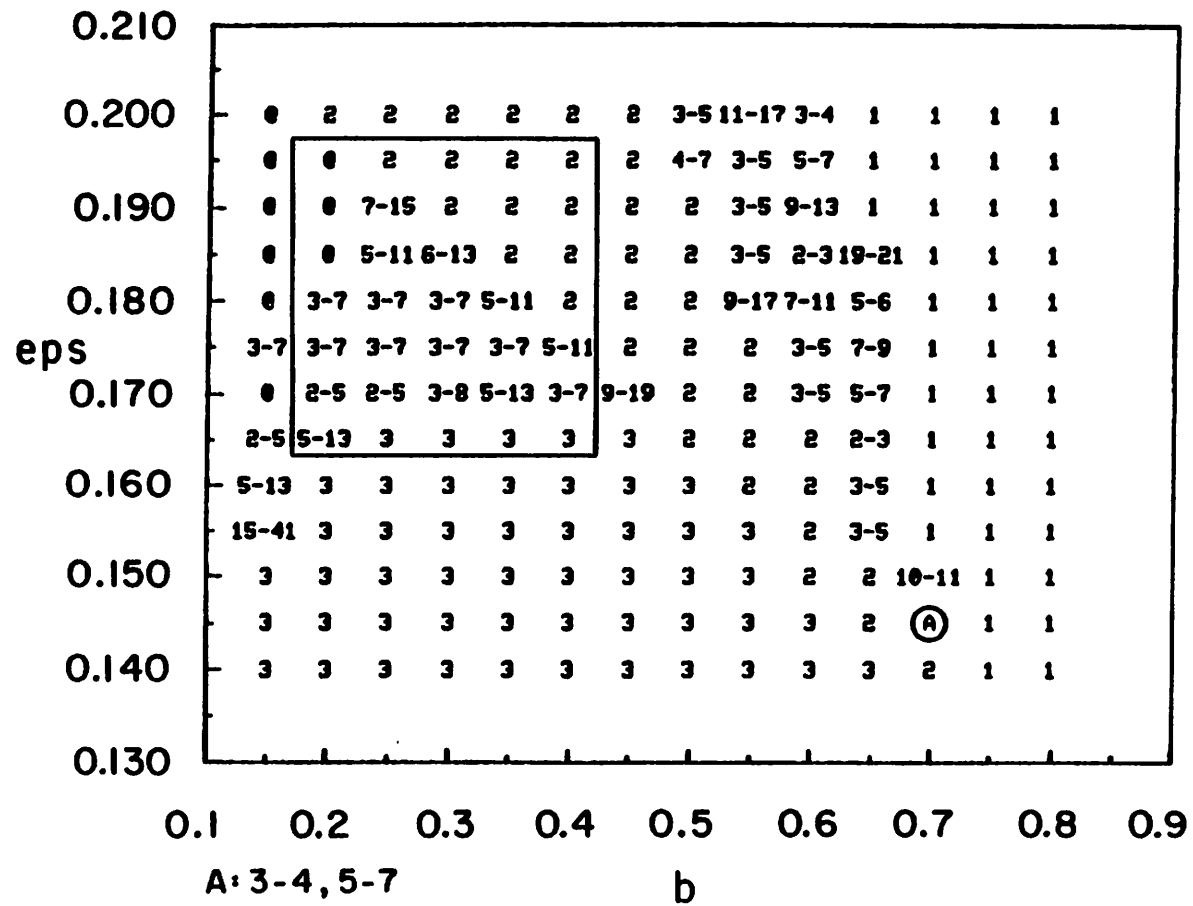
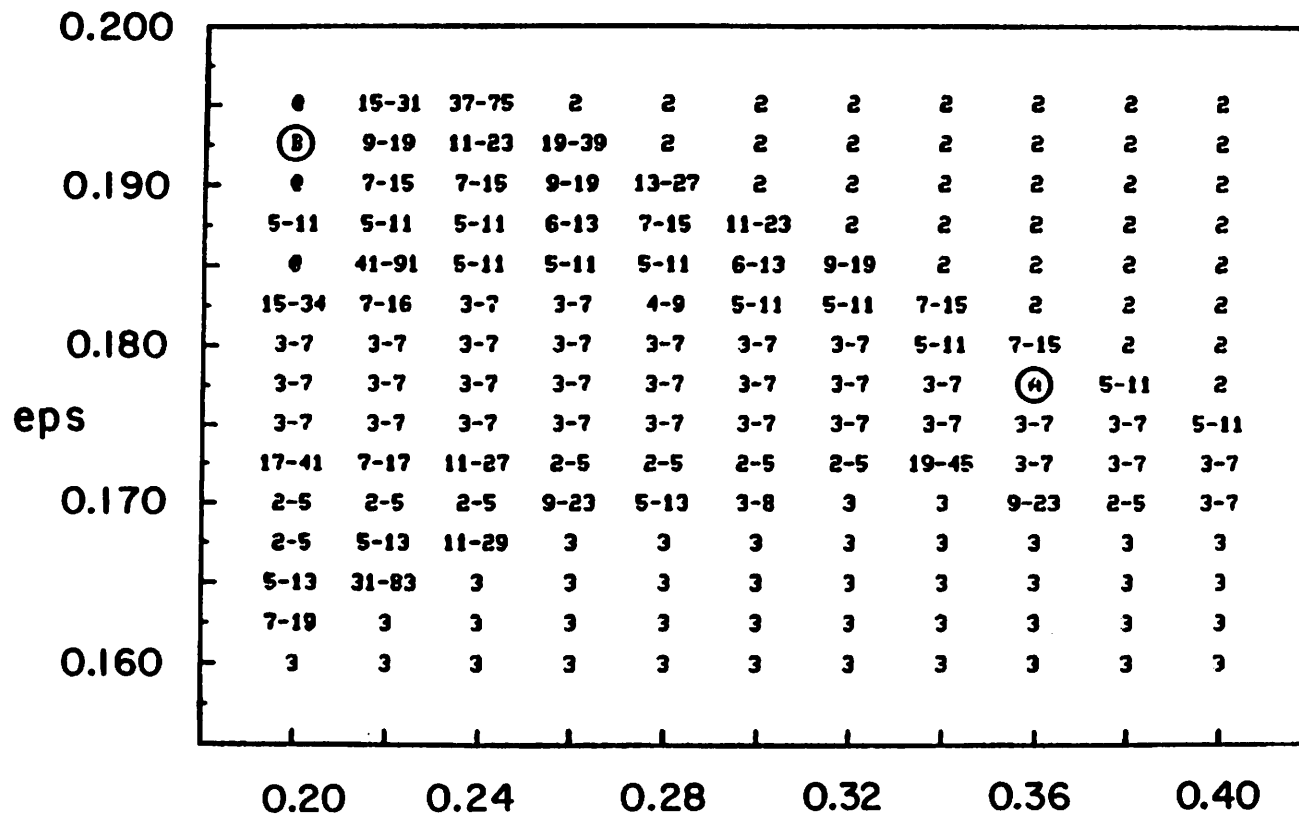


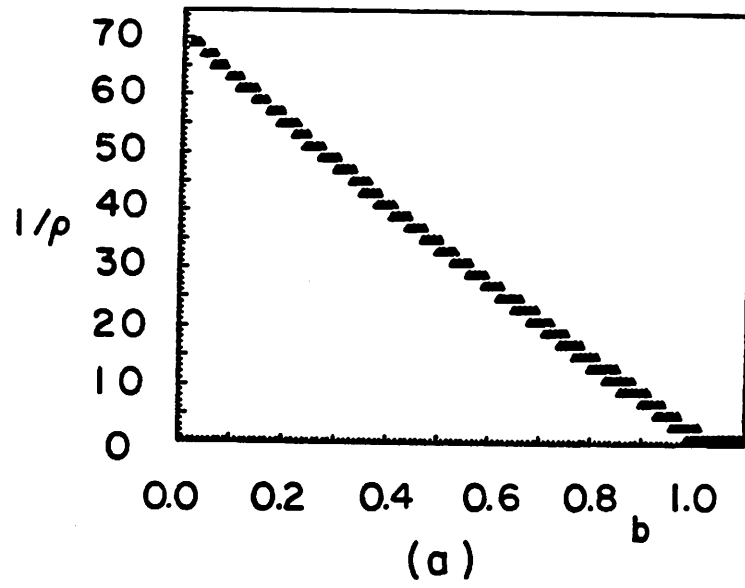
Fig.6(b)



A: 4-9, 39-90
 B: 42-89, ⓐ

Fig.6(c)

eps = 0.005



eps = 0.0025

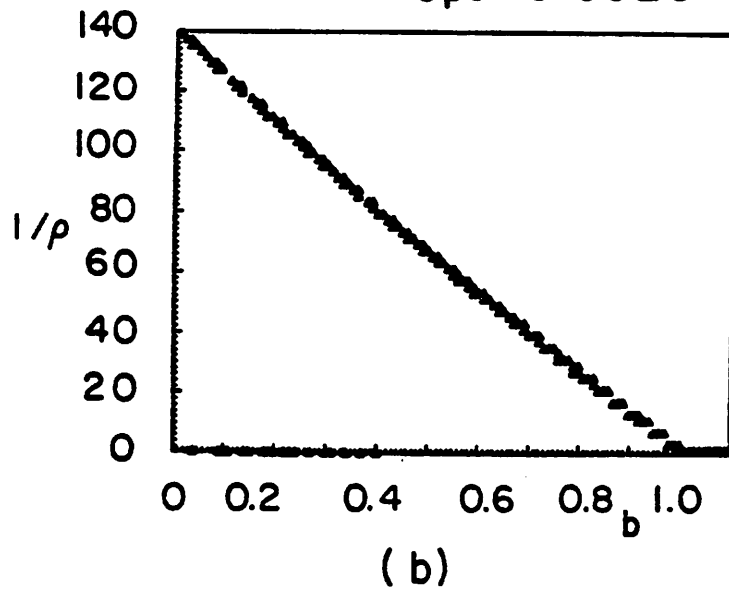


Fig. 7

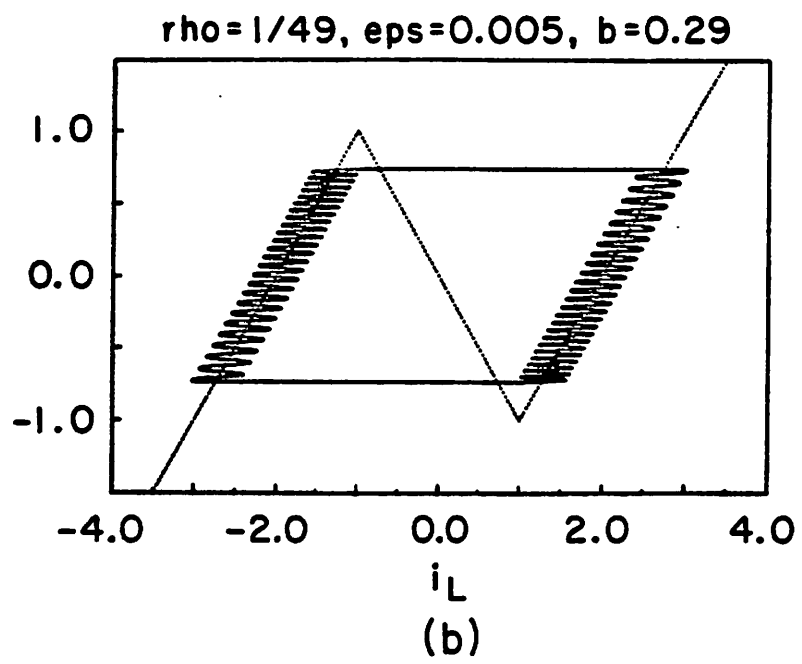
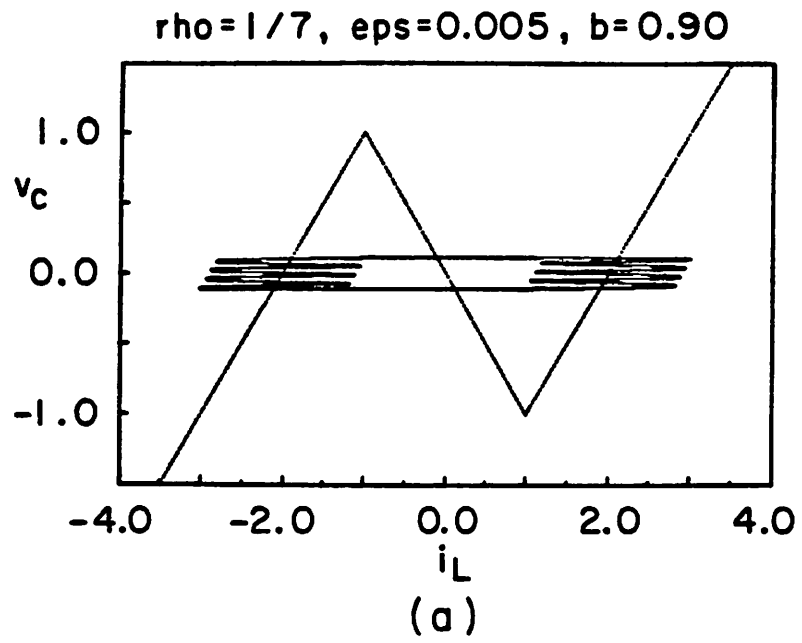
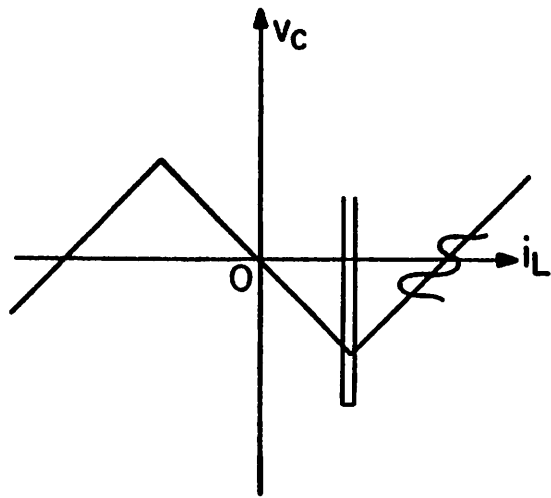
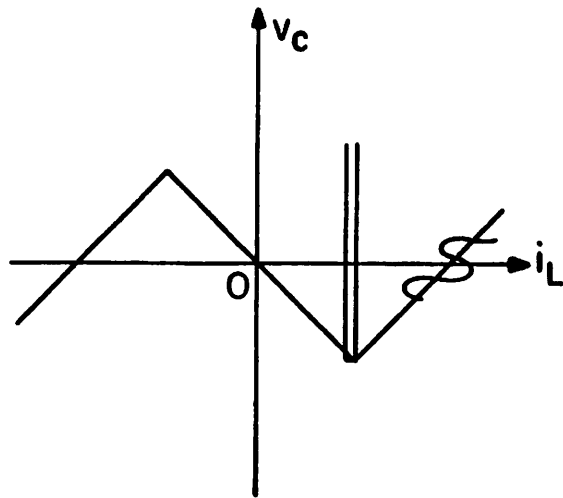


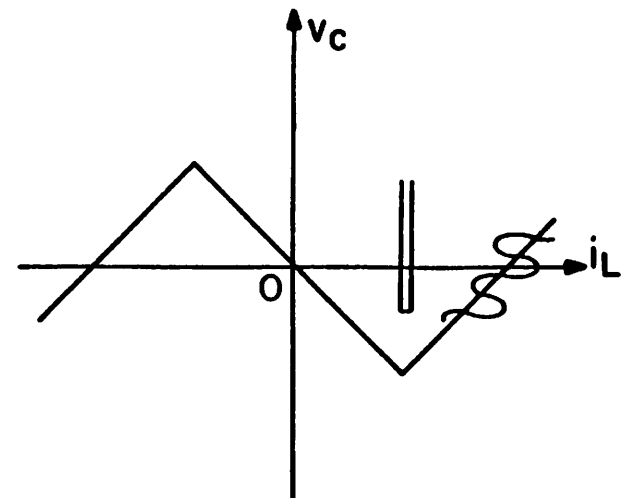
Fig. 8



(a)



(b)



(c)

Fig. 9

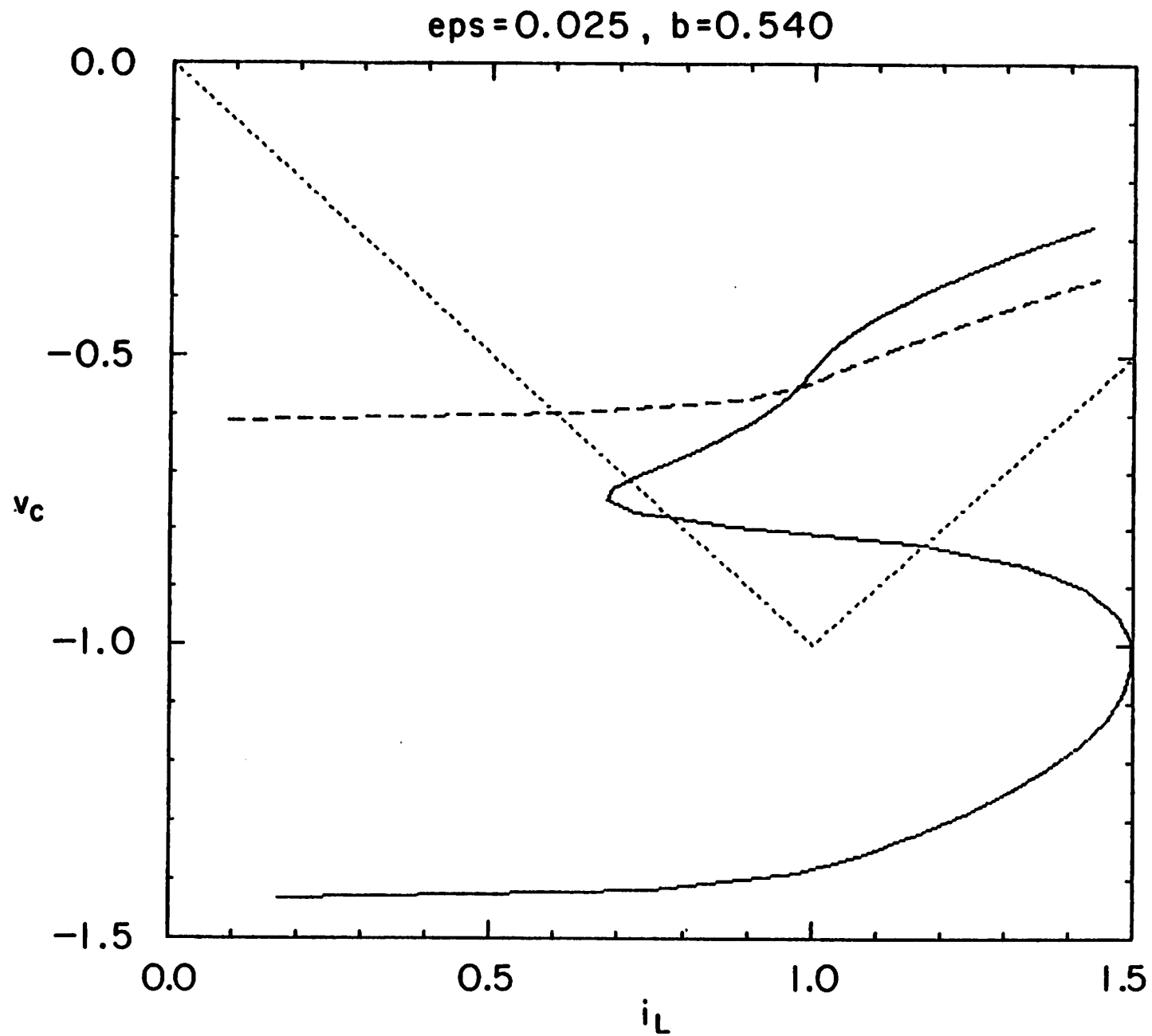


Fig. 10

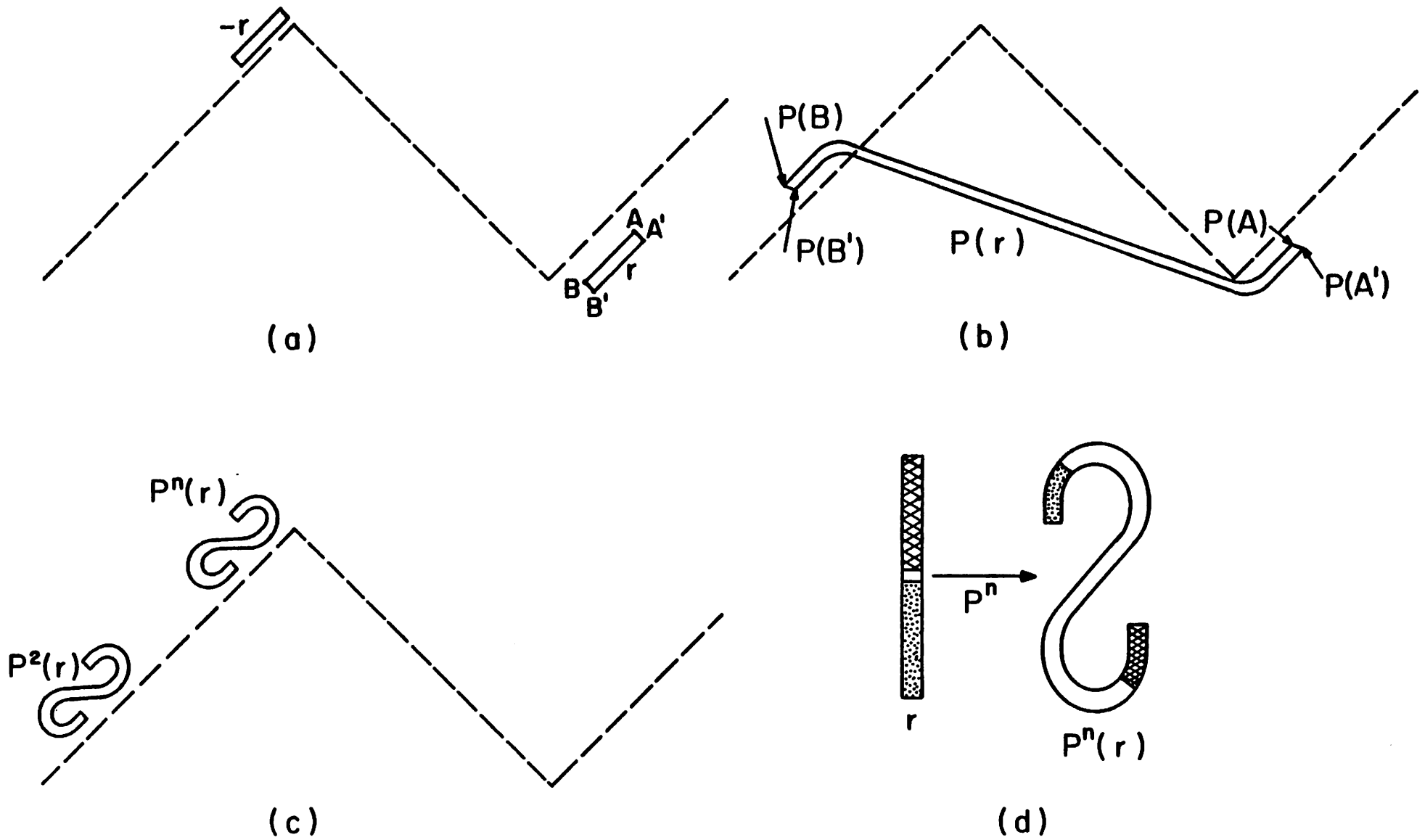
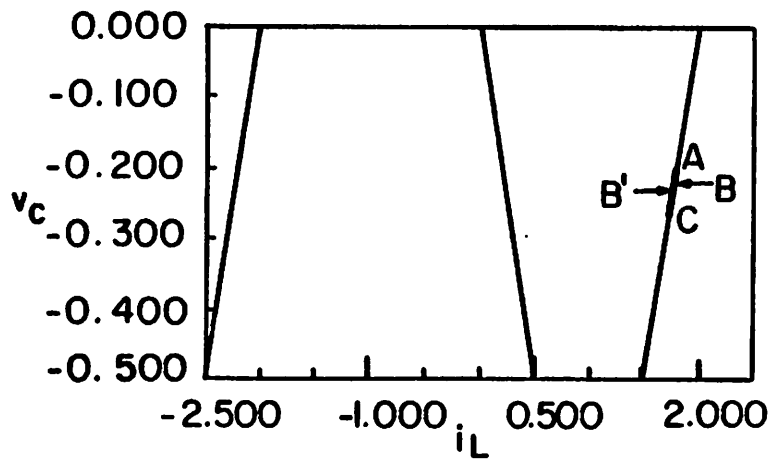
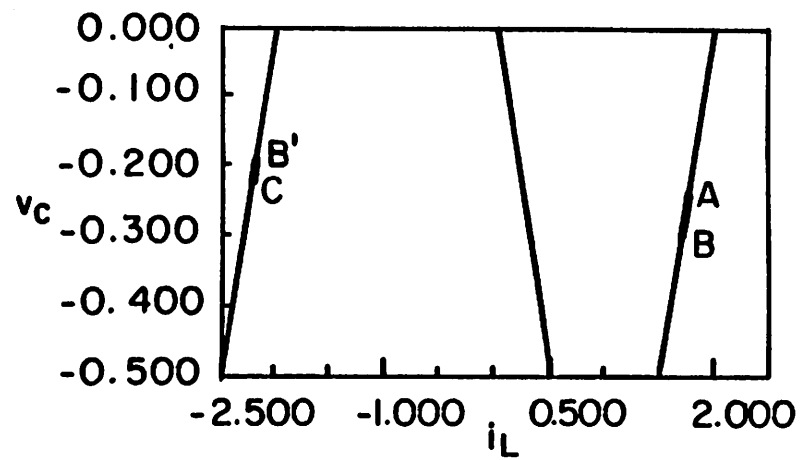


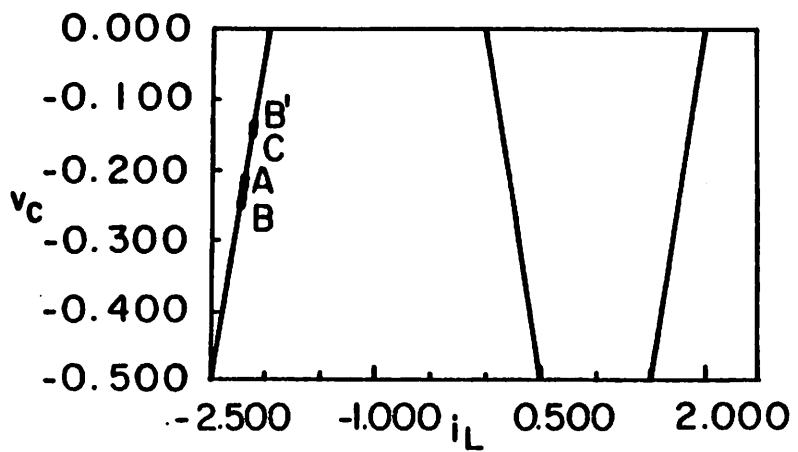
Fig. 11



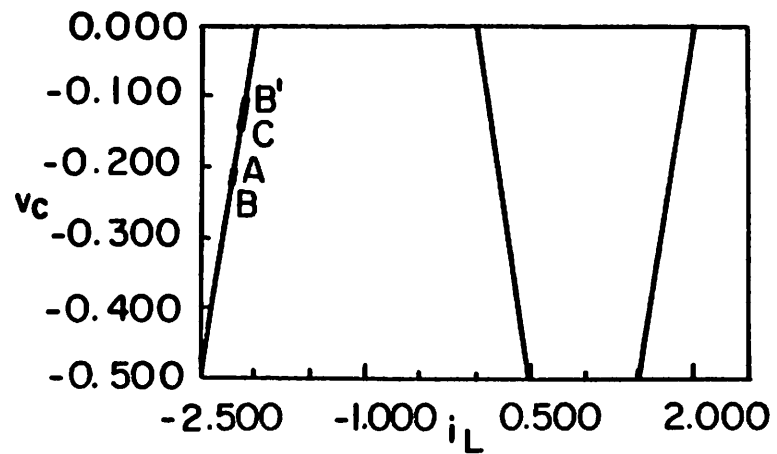
(a)



(b)



(c)



(d)

Fig. 12

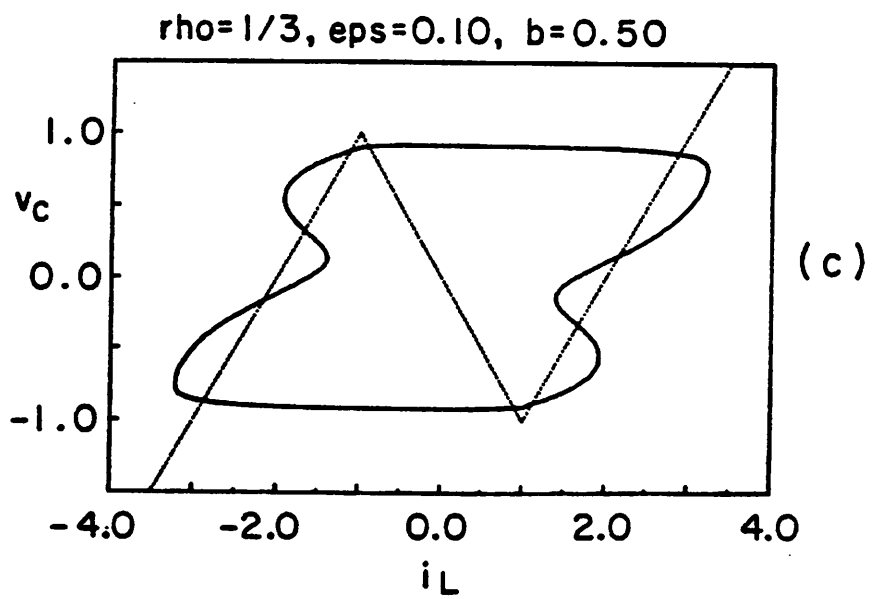
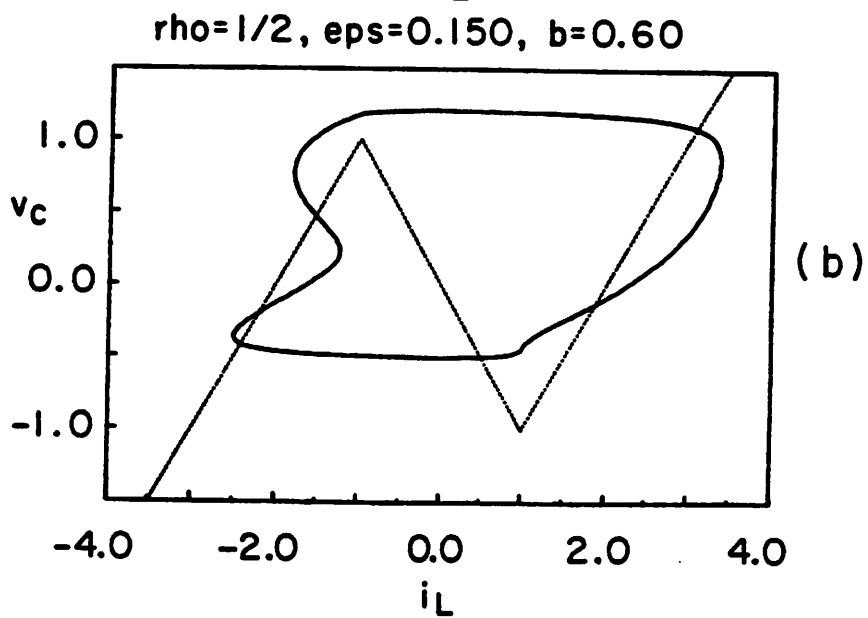
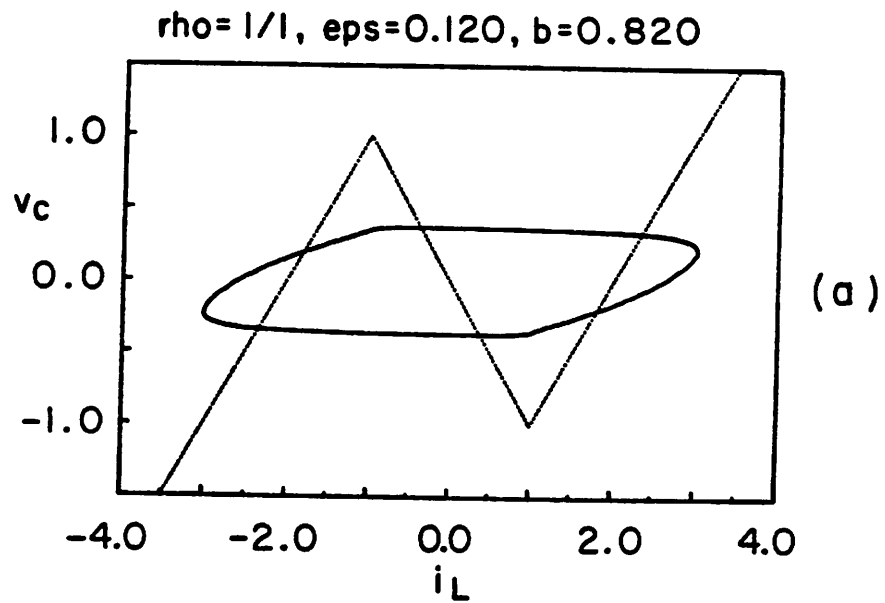


Fig. 13

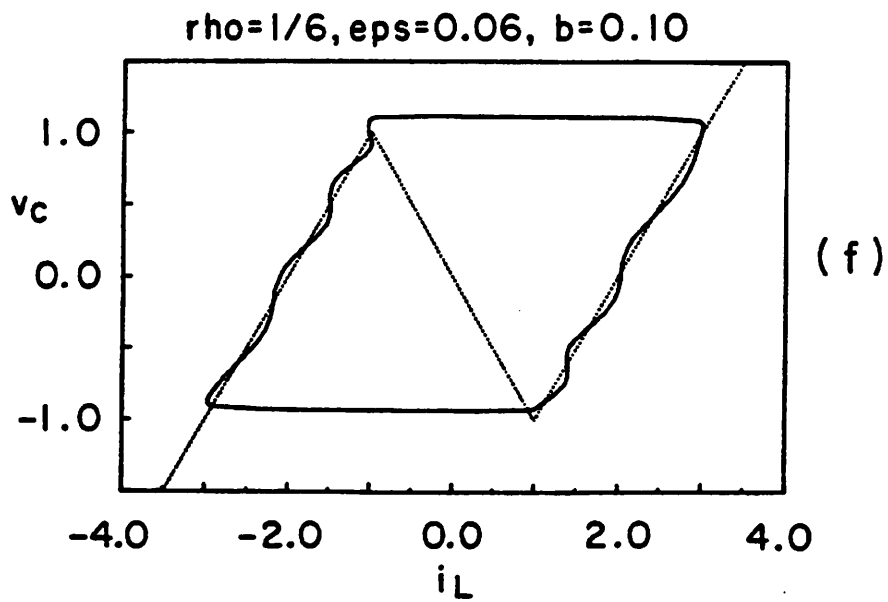
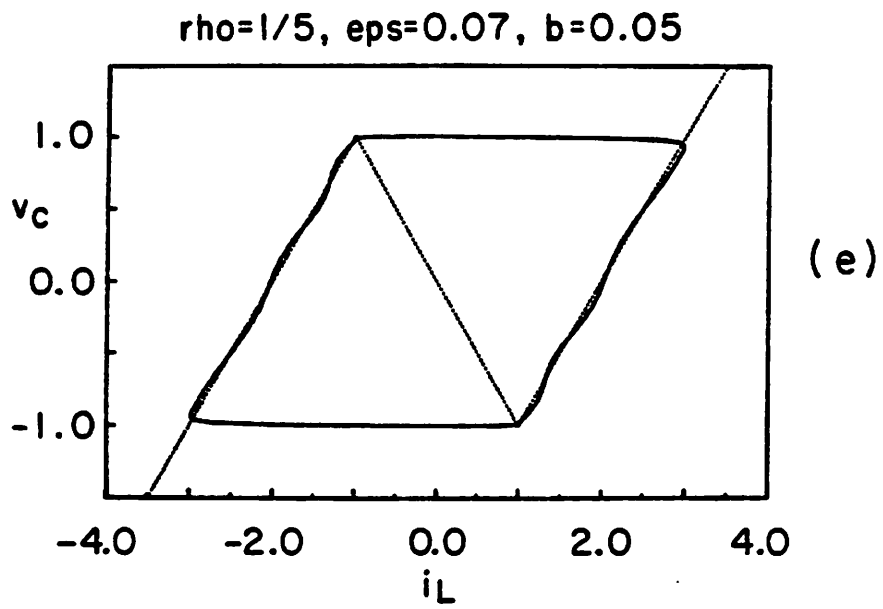
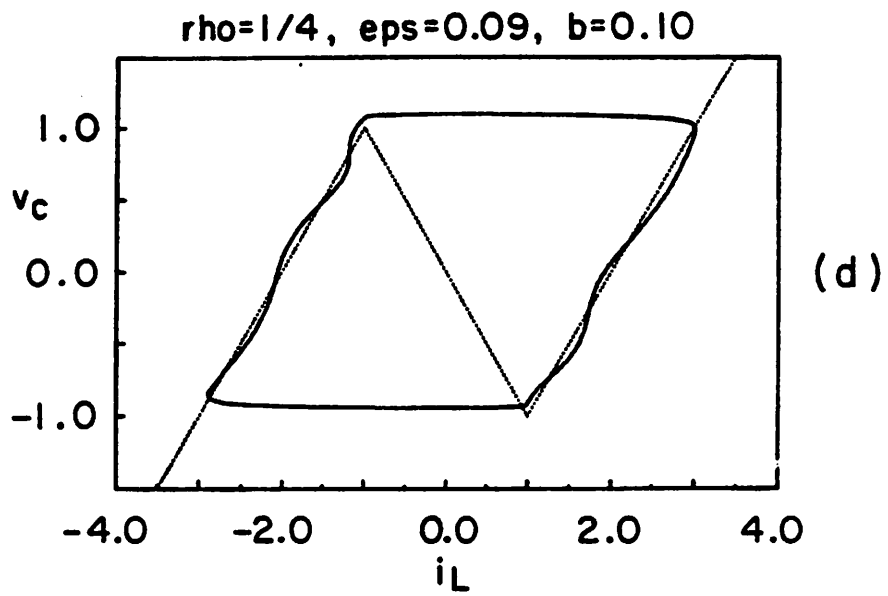


Fig. 13 (cont'd)

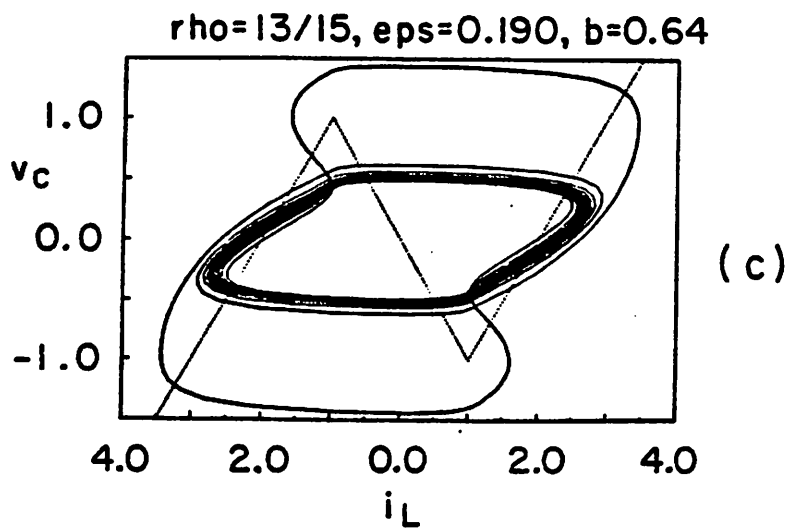
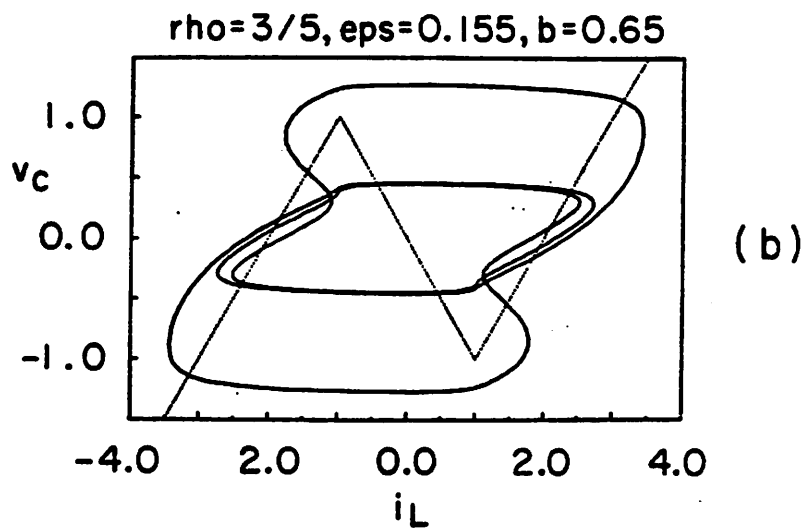
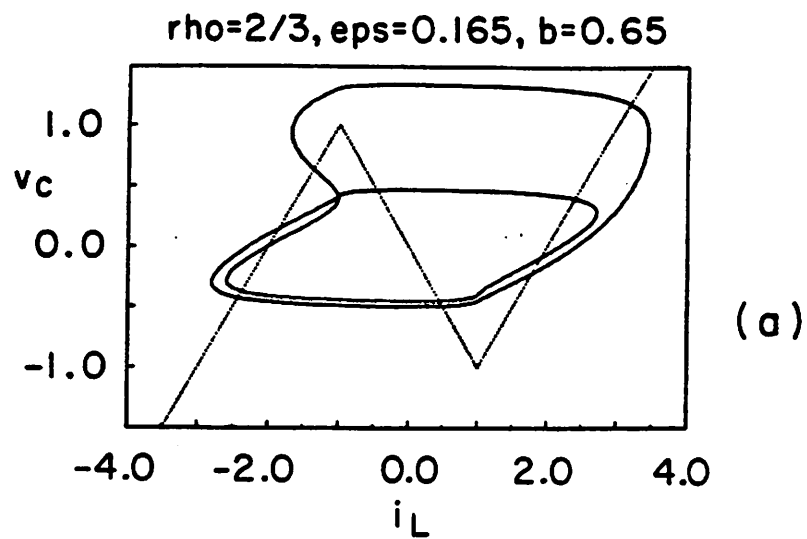
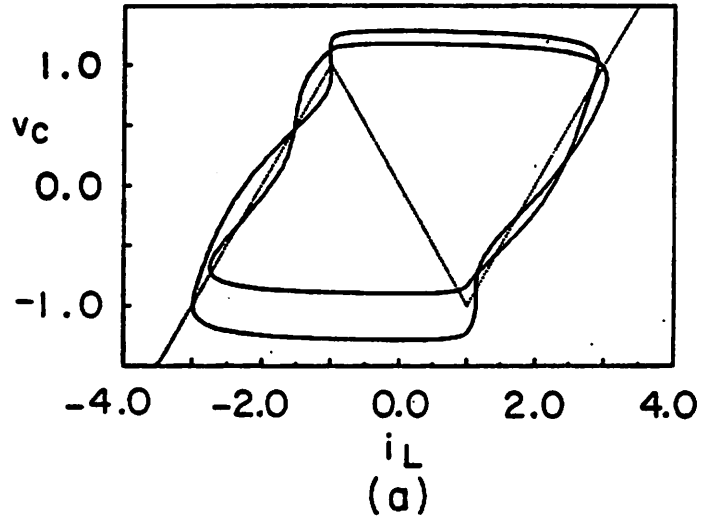


Fig. 14

$\rho=2/5, \epsilon=0.170, b=0.20$



$\rho=4/9, \epsilon=0.1825, b=0.28$

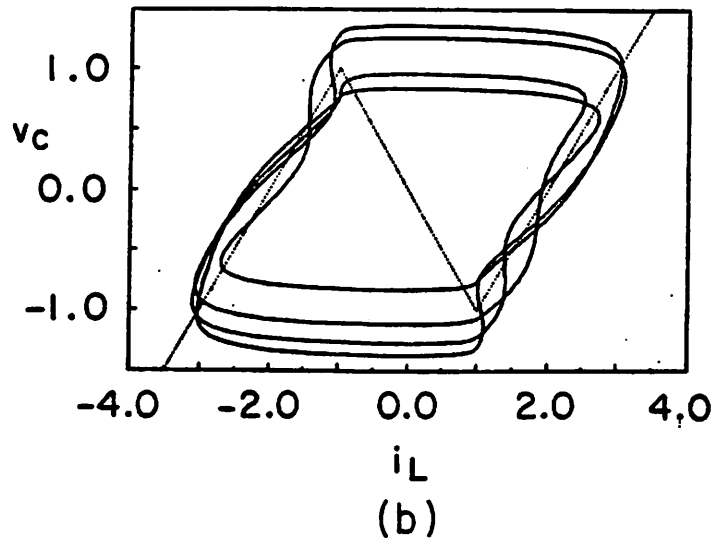


Fig. 15

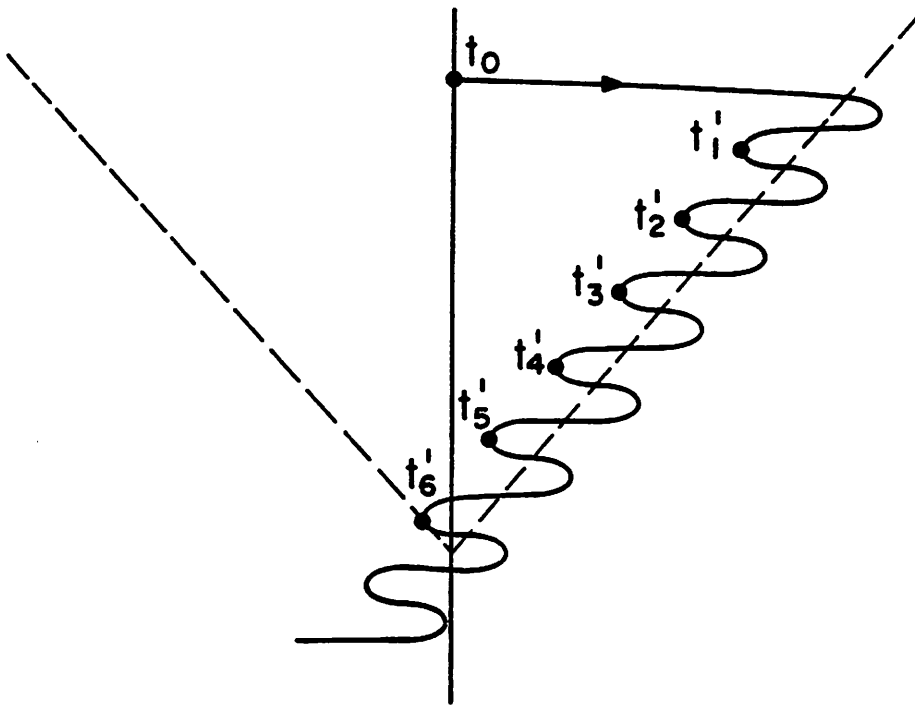
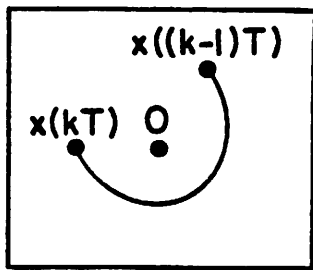
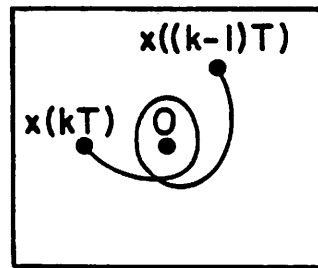


Fig. I.I



allowed

(a)



disallowed

(b)

Fig. IV.I